AGU PUBLICATIONS

JGR

Journal of Geophysical Research: Atmospheres

RESEARCH ARTICLE

10.1002/2016JD024834

Key Points:
- VIIRS is the mainstay polar-orbiting sensor, and its aerosol products are the primary global aerosol data once the EOS end their missions
- VIIRS AOT and Ångström Exponent EDR are compared with AERONET L2.0 to determine their Validated Stage maturity level
- All metrics, including newly defined expected error, provide evidence that VIIRS aerosol products are of high quality

Correspondence to:
J. Huang,
jingfeng.huang@noaa.gov

Citation:
Huang, J., S. Kondragunta, I. Laszlo, H. Liu, L. A. Remer, H. Zhang, S. Superczynski, P. Ciren, B. N. Holben, and M. Petrenko (2016), Validation and expected error estimation of Suomi-NPP VIIRS aerosol optical thickness and Ångström exponent with AERONET, *J. Geophys. Res. Atmos.*, *121*, 7139–7160, doi:10.1002/2016JD024834.

Received 21 JAN 2016
Accepted 18 MAY 2016
Accepted article online 20 MAY 2016
Published online 23 JUN 2016

©2016. American Geophysical Union. All Rights Reserved.

Validation and expected error estimation of Suomi-NPP VIIRS aerosol optical thickness and Ångström exponent with AERONET

Jingfeng Huang[1,2], Shobha Kondragunta[2], Istvan Laszlo[2,3], Hongqing Liu[2,4], Lorraine A. Remer[5], Hai Zhang[2,4], Stephen Superczynski[2,6], Pubu Ciren[2,4], Brent N. Holben[7], and Maksym Petrenko[7,8]

[1]Earth System Science Interdisciplinary Center, University of Maryland, College Park, Maryland, USA, [2]Center for Satellite Applications and Research, National Oceanic and Atmospheric Administration, National Environmental Satellite, Data, and Information Service, College Park, Maryland, USA, [3]Department of Atmospheric and Oceanic Science, University of Maryland, College Park, Maryland, USA, [4]I. M. Systems Group, Inc., College Park, Maryland, USA, [5]Joint Center for Earth Systems Technology, University of Maryland, Baltimore, Maryland, USA, [6]Systems Research Group, College Park, Maryland, USA, [7]NASA Goddard Space Flight Center, Greenbelt, Maryland, USA, [8]ADNET Systems Inc., Bethesda, Maryland, USA

Abstract The new-generation polar-orbiting operational environmental sensor, the Visible Infrared Imaging Radiometer Suite (VIIRS) on board the Suomi National Polar-orbiting Partnership (S-NPP) satellite, provides critical daily global aerosol observations. As older satellite sensors age out, the VIIRS aerosol product will become the primary observational source for global assessments of aerosol emission and transport, aerosol meteorological and climatic effects, air quality monitoring, and public health. To prove their validity and to assess their maturity level, the VIIRS aerosol products were compared to the spatiotemporally matched Aerosol Robotic Network (AERONET) measurements. Over land, the VIIRS aerosol optical thickness (AOT) environmental data record (EDR) exhibits an overall global bias against AERONET of −0.0008 with root-mean-square error (RMSE) of the biases as 0.12. Over ocean, the mean bias of VIIRS AOT EDR is 0.02 with RMSE of the biases as 0.06. The mean bias of VIIRS Ocean Ångström Exponent (AE) EDR is 0.12 with RMSE of the biases as 0.57. The matchups between each product and its AERONET counterpart allow estimates of expected error in each case. Increased uncertainty in the VIIRS AOT and AE products is linked to specific regions, seasons, surface characteristics, and aerosol types, suggesting opportunity for future modifications as understanding of algorithm assumptions improves. Based on the assessment, the VIIRS AOT EDR over land reached Validated maturity beginning 23 January 2013; the AOT EDR and AE EDR over ocean reached Validated maturity beginning 2 May 2012, excluding the processing error period 15 October to 27 November 2012. These findings demonstrate the integrity and usefulness of the VIIRS aerosol products that will transition from S-NPP to future polar-orbiting environmental satellites in the decades to come and become the standard global aerosol data set as the previous generations' missions come to an end.

1. Introduction

Atmospheric aerosols, small solid and liquid particles suspended in the air, are introduced into the atmosphere from natural and anthropogenic sources and include mineral dust, biomass burning smoke, volcanic ash, industrial pollutants, sea salt, and biogenic compounds. Not only are some of these particles detrimental to human health [*Pope et al*., 2002] and contribute to visibility impairment [*Hand et al*., 2011], they also affect local and global water and energy cycles and atmospheric chemistry [*Ramanathan et al*., 2001; *Rosenfeld et al*., 2008; *Chin et al*., 2009; *Koren and Feingold*, 2011; *Koren et al*., 2012; *Martin et al*., 2003]. Aerosols are active constituents in Earth's radiative balance, scattering, and absorbing solar radiation, which contribute to global climate forcing [*Lau et al*., 2006; *Chin et al*., 2009]. Because aerosols act as cloud condensation nuclei and because of their radiative effects, they can induce changes in cloud formation and lifetime [*Albrecht*, 1989; *Twomey*, 1977], systematically delay the formation and development of precipitation [*Guo et al*., 2015], and thus impact rainfall and hydrological cycles [*Ramanathan et al*., 2001; *Lohmann and Feichter*, 2005; *Rosenfeld et al*., 2008; *Koren and Feingold*, 2011; *Koren et al*., 2012]. Aerosol also influences biogeochemical cycles. For example, the Trans-Atlantic African dust deposition over the Amazon Basin provides important nutritional supply to the Amazon rainforest [e.g., *Yu et al*., 2015].

While aerosol forcing may offset some of the warming caused by greenhouse gases in the atmosphere, quantifying that offset with confidence continues to be one of the daunting environmental challenges currently faced by the research community [*Boucher et al*., 2013]. Furthermore, the capability to predict future climate:

temperature, cloud, and precipitation distributions, is severely hampered by a lack of understanding of the role of aerosols in these systems [*Chin et al*., 2009]. The difficulty is in understanding the role of aerosols within complex meteorological and climatological processes. Aerosols themselves are complex substances originating from various emission sources as varied as deserts, wild fires, and fossil fuel combustion [*Streets et al*., 2003; *Ginoux et al*., 2012]. Then the original substances evolve and age during transport and dispersion, changing their chemical, physical, and optical properties over time scales of minutes to days [*Chin et al*., 2009; *Yu et al*., 2013]. Modeling these myriad processes, across all scales, is required for better understanding of the processes leading to better predictive capability, but the models must be constrained, supported, and validated by comprehensive observation-based data sets. Data assimilation of satellite aerosol observations improves numerical model predictions by accounting for inaccuracies in model sources and sinks. Numerical model prediction of aerosols with better accuracy is used to provide air quality forecast guidance. The operational NOAA National Weather Service and Environmental Protection Agency National Air Quality Forecast system (http://airquality.weather.gov/) and the Naval Research Laboratory Aerosol Analysis and Prediction System [*Zhang et al*., 2014] are two specific examples of assimilation systems that ingest satellite aerosol products. Assimilation systems require confident estimates of data uncertainty and expected errors of the products used as inputs.

On the global scale spaceborne sensors provide the best spatial and temporal coverage of the aerosol system [*King et al*., 1999; *Diner et al*., 2004], but the complexities in the aerosol physiochemical and optical properties impose great challenges and introduce large uncertainty [*Kaufman et al*., 1997, 2002; *Diner et al*., 2004; *Myhre et al*., 2005; *Chin et al*., 2009]. Therefore, comprehensive and systematic validation of satellite aerosol retrievals using high-quality ground measurements is essential for scientific and operational applications of satellite aerosol products.

For over 15 years, the Moderate Resolution Imaging Spectroradiometer (MODIS) and the Multiangle Imaging SpectroRadiometer (MISR) on board the NASA Earth Observing System satellites Terra and Aqua have provided quality global aerosol observations [*Kaufman et al*., 1997, 2002; *Remer et al*., 2005, 2008; *Levy et al*., 2007, 2010, 2013; *Sayer et al*., 2013; *Hsu et al*., 2013; *Kahn et al*., 2010]. These heritage satellite aerosol products were validated, and their expected error was estimated using Aerosol Robotic Network (AERONET) ground measurements as truth for collocated satellite retrievals. These validation exercises were able to quantify the expected uncertainty or expected error of an individual retrieval, distributed randomly within the global data set. The quantification of expected error is a fundamental metric of a satellite aerosol product, necessary for acceptance by the aerosol community.

The heritage polar-orbital sensors MODIS and MISR are nearing the end of their lifespans. To continue this heritage of global Earth observations, the Suomi National Polar-orbiting Partnership (S-NPP), which is the first satellite in the series of the United States' next generation polar-orbiting operational environmental satellite system, the Joint Polar Satellite System (JPSS), was launched on 28 October 2011. This series of satellites will carry a variety of sensors that will observe the Earth system and derive a wide array of parameters that characterize the terrestrial surface, the oceans, and the atmosphere [*Goldberg*, 2013]. Critical daily global aerosol products, similar to those traditionally provided by MODIS at near-daily global coverage, are now being produced from observations of the Visible Infrared Imaging Radiometer Suite (VIIRS), one of the instruments onboard S-NPP, but with much wider swath widths leaving no data gap in daily global observations. Due to its wider swath width, VIIRS does not have orbital gaps near the equator as MODIS does and captures aerosol plumes better at the edge of the scan that MODIS occasionally misses. Thus, after the demise of MODIS, VIIRS will be the primary source of observationally based global aerosol data essential for a wide range of applications.

The VIIRS aerosol data products are derived primarily from the radiometric channels covering the visible through the short-wave infrared spectral regions (412 nm to 2250 nm [*Jackson et al*., 2013]). The product includes AOT at a pixel level (~750 m) and is considered an intermediate product (IP) to the AOT environmental data record (EDR) at ~6 km resolution, which is aggregated from the finer-resolution IP product. The VIIRS aerosol algorithm also retrieves Ångström Exponent (AE) referred to as aerosol particle size parameter and outputs AOT at 11 different wavelengths from 412 nm to 2250 nm. This paper presents the validation of the EDR and IP AOT products over land and the EDR and IP AOT and AE products over ocean. These are the most commonly used aerosol parameters for climate and weather forecasting modeling and other community-wide applications. Similar to MODIS [*Levy et al*., 2013], our evaluation also indicated that the VIIRS AE product over land currently has no quantitative value. Therefore, the evaluation of the VIIRS AE over land is not included in this paper.

The calibration and validation (Cal/Val) of the VIIRS aerosol algorithm and products go through the following phases: prelaunch Cal/Val, early orbit checkout, intensive Cal/Val that assesses beta and provisional maturity of the products, and long-term monitoring once the products reach validated stage. At the provisional stage of the VIIRS aerosol products, initial evaluation of VIIRS EDR AOT was made by comparing the product with Aqua MODIS retrievals and measurements from AERONET and the Maritime Aerosol Network (MAN) [*Liu et al*., 2014]. This preliminary evaluation period covered the time from 2 May 2012 to 1 September 2013 and used the near-real-time Level 1.5 AERONET Direct Sun measurements [*Liu et al*., 2014] due to the lack of the quality assured Level 2.0 AERONET measurement at that time. Since then, with an extended temporal coverage of VIIRS aerosol products, more quality assured AERONET L2.0 direct-Sun products have become available for a more extensive assessment.

In this paper we perform an extensive comparison of VIIRS aerosol products to AERONET observations. We will assess the accuracy and uncertainty of the products and estimate expected errors. This will be the first time expected error is estimated for the VIIRS products. Section 2 briefly describes the VIIRS AOT algorithm and the data sets used in this study, the validation approach, and defines the statistical parameters used to quantify the quality of the product. Sections 3 and 4 present the validation results and the expected error estimation, respectively. Section 5 summarizes the study with discussion.

2. VIIRS Aerosol Product and Validation Approaches

2.1. VIIRS Aerosol Algorithm

The VIIRS aerosol algorithm is based on the MODIS heritage. Details of the algorithm can be found in *Jackson et al*. [2013], the VIIRS Aerosol Products Algorithm Theoretical Basis Document [*Aerosol ATBD*, 2015a], and the Operational Algorithm Description document [*Aerosol OAD*, 2015b].

Like MODIS, the VIIRS products are produced by two separate algorithms, one applied over land surfaces and one applied over oceans. The VIIRS over land algorithm is based on the MODIS atmospheric correction algorithm [*Kotchenova and Vermote*, 2007; *Vermote and Kotchenova*, 2008]. Prescribed look-up tables (LUTs) were produced by the Second Simulation of a Satellite Signal in the Solar Spectral Vector code [*Vermote et al*., 1997; *Kotchenova et al*. 2006] with different viewing geometries, different AOT values, and five land aerosol models. Spectral surface reflectance ratios were also prescribed at selected visible and infrared bands. The optimal AOT is selected by finding the minimum residuals between the calculated and the prescribed surface reflectance ratios [*Jackson et al*., 2013].

The VIIRS over ocean algorithm originates from the operational MODIS over-ocean retrieval [*Tanré et al*., 1997; *Remer et al*., 2009; *Levy et al*., 2013]. There are four fine mode and five coarse mode aerosol models in the ocean aerosol algorithm. The VIIRS ocean aerosol algorithm finds the optimal pair of one fine mode and one coarse mode aerosol models that can closely match the measured and the calculated top-of-atmosphere reflectance at multiple selected spectral bands. The algorithm returns the AOT, the choice of each mode, and the relative weight of each mode, called the Fine Mode Fraction. From this information, the full spectral AOT can be obtained and various aerosol particle size parameters can be determined.

2.2. VIIRS Aerosol Products

Only the VIIRS AOT and AE EDRs are validated in this study. Because of a significant improvement in the VIIRS land AOT owing to an update of the prescribed surface reflectance ratios on 22 January 2013 [*Liu et al*., 2014], the validation period for the VIIRS land AOT was selected from 23 January 2013 to 31 December 2014. Over ocean, however, the VIIRS aerosol algorithm did not significantly change since 2 May 2012. Therefore, the validation period for the VIIRS Ocean AOT and AE EDR extends from 2 May 2012 to 31 December 2014, except for the period from 15 October 2012 to 27 November 2012 that is excluded due to an error in the processing. Although the VIIRS Aerosol EDR reports AOT at 11 spectral wavelengths, the primary AOT product evaluated in this study is the AOT at 550 nm (AOT hereafter unless otherwise noted). Only the operational VIIRS ocean AE product calculated from the spectral AOT at 865 nm and 1610 nm is evaluated in this study.

Although the IP retrievals are not an official product that requires assessment for validated stages, their ~750 m at nadir spatial resolution is useful for the air quality user community and other users who require high-resolution aerosol imagery for qualitative evaluation and monitoring of aerosol events. Therefore, we also compare the VIIRS IP AOT and AE products with AERONET observations to evaluate data accuracy and

uncertainty and report findings here for reference. For AOT, the VIIRS Aerosol IP product only reports AOT at one wavelength, 550 nm. For AE, only the Ocean AE IP calculated at 865 nm and 1610 nm is evaluated in this study.

2.3. Validation Approach With AERONET

The AERONET network provides a long-term, continuous, and readily accessible database of aerosol optical properties in the public domain for validation of satellite retrievals [http://aeronet.gsfc.nasa.gov, *Holben et al*., 1998]. The near-real-time Level 1.5 data sets offer a means for quick evaluation of a satellite product. The AERONET Level 2.0 data sets undergo greater quality assurance procedures including temporal variability checking and postdeployment calibration. Thus, the Level 2.0 products are recommended for satellite data validation purposes [*Smirnov et al*., 2000].

For this study, only the Level 2.0 AERONET Direct Sun Algorithm AOT products at 10 spectral wavelengths are used to interpolate AOT values to 11 VIIRS wavelengths. The interpolation uses a second-order polynomial fitting of AERONET AOT and wavelengths in logarithmic coordinates with all available AERONET measurements at wavelengths from 340 nm to 870 nm plus 1640 nm [*Eck et al*., 1999; *Remer et al*., 2005; *Levy et al*., 2010; *Kahn et al*., 2010]. The AERONET measurements at 1020 nm are not used due to their relatively larger data uncertainty attributable to water vapor absorption and the temperature sensitivity of the detector at 1020 nm (Tom Eck, personal communication). Use of multiple channels minimizes the uncertainty of any single channel in interpolating to another wavelength [*Eck et al*., 1999]. The established second-order polynomial relation between AERONET AOT and wavelengths in logarithmic coordinates is then used to calculate AOT values at 11 VIIRS wavelengths from 412 nm to 2250 nm to be compared to the VIIRS spectral AOT at the same corresponding wavelength.

This study conducted the multisensor aerosol product matching up using the Multisensor Aerosol Products Sampling System (MAPSS). The MAPSS was developed at the NASA Goddard Space Flight Center. The system consistently samples and generates the spatial statistics of aerosol products from multiple spaceborne sensors, including the Moderate Resolution Imaging Spectroradiometer (MODIS), the Multiangle Imaging SpectroRadiometer (MISR), the Ozone Monitoring Instrument, the Polarization and Directionality of Earth Reflectances, and the Cloud-Aerosol Lidar and Infrared Pathfinder Satellite Observations, enabling a direct cross characterization and data integration between on-orbit aerosol observations from multiple sensors and providing well-characterized collocated data for the integrated validation of satellite aerosol products [*Petrenko et al*., 2012]. The latest development of the system includes the VIIRS EDR aerosol products. For each MAPSS-generated VIIRS EDR-AERONET matchup, the corresponding VIIRS IP retrievals are added to the matchup for the VIIRS IP evaluation purposes.

For the VIIRS versus AERONET matchup, the spatial statistics of the satellite retrieval are calculated for a 27.5 km circle, centered at the AERONET station. The best quality assured VIIRS retrievals are averaged within the circle to represent the value of the satellite product for that collocation. Correspondingly, temporal statistics of the AERONET measurements are calculated for a one-hour time window (±30 min of satellite overpass time) for the same collocation. The matchup scheme requires at least 20% of all the possible VIIRS retrievals (~15 VIIRS EDR retrievals at nadir) within the 27.5 km radius circle to be of high quality and at least two AERONET measurements to be available during the one-hour time window. When VIIRS pixels are spatially averaged to matchup with AERONET station, the best quality land and ocean retrievals within the spatial domains are averaged separately. If the number of best quality land or ocean retrievals meets the sampling requirements, the matchups are used for the land or ocean validation respectively. More information about MAPSS can be found in *Petrenko et al*. [2012] and at the MAPSS website http://disc.gsfc.nasa.gov/aerosols/services/mapss/ (accessed on 02 December 2015).

2.4. Statistical Parameters for Validation and Expected Error Estimation

Several key parameters are defined for VIIRS aerosol product validation. Accuracy is the mean of the biases between the VIIRS aerosol retrievals and the AERONET ground measurements. Precision is the standard deviation of the biases while uncertainty is the root-mean-square error of the biases, both of which are indicative of noise in the data and describe how far the VIIRS retrievals have deviated from AERONET measurements in both positive and negative directions. The smaller the accuracy, the uncertainty, or the

precision, the closer the VIIRS versus AERONET matchup data pairs are to the 1:1 line in the scatterplot, and the better the performance of the satellite retrievals.

For expected error estimation, the evaluation of the heritage satellite aerosol products adopted a conventional approach that the expected error bars should enclose 1 standard deviation of all retrievals based on the assumption that the biases should follow a Gaussian distribution. The expected errors are derived from the two linear envelopes above and below the 1:1 line on a scatterplot that embraces at least 68% (approximately 1 standard deviation) of the matchups [*Levy et al*., 2013; *Sayer et al*., 2013].

However, during the expected error evaluation, we found that the bias distributions are not always Gaussian. This means, if we want to describe expected error more precisely, expected error should count both how far the mean biases are away from the truth (expected accuracy, EA) and how much individual retrievals fluctuate from the mean biases (expected precision, EP). Moreover, expected errors have strong dependence on actual aerosol loading. Therefore, we will estimate expected errors as functions of either AERONET measurements or VIIRS observations. The former function is useful for expected error calculation when truth is known. But for most satellite retrievals without AERONET sites in adjacency, the latter function will be valuable to have approximate estimation of errors based on satellite retrievals.

3. Validation Results

3.1. Time Series of VIIRS AOT EDR Versus AERONET

To obtain an overall view of the difference between the VIIRS EDR and AERONET in terms of mean global AOT, we plot the time series of this parameter as shown in Figure 1, for land and ocean, respectively. Based on the VIIRS-AERONET matchup data set, the VIIRS and AERONET AOT means averaged over all the matchups at each calendar day were compared and their differences calculated. Only collocated data are included in the time series.

As illustrated in Figure 1a, the daily AOT variations and their seasonality, observed by the VIIRS Land AOT EDR and AERONET for the period of 23 January 2013 to 31 December 2014, are similar. Both indicate higher AOT during the northern hemisphere summer and lower AOT during winter. There is, however, evidence of a significant seasonal variability in the bias with positive biases in boreal summer and negative biases in boreal winter (Figure 1b). Some of these biases are attributed to the retrieval assumption that treats the spectral surface reflectance ratios (412 nm, 445 nm, or 488 nm over 672 nm) as constants globally while these ratios actually have some dependence on seasonal surface characteristics, such as seasonally varying vegetation growth and senescence [*Liu et al*., 2014].

Agreements between the VIIRS Ocean AOT EDR and AERONET are shown in Figure 1c over the data period of 02 May 2012 to 31 December 2014 with the processing error period 15 October 2012 to 27 November 2012 excluded. Although the seasonal variability in the daily and monthly AOT mean differences are not as significant as observed in the land counterpart, the VIIRS Ocean AOT EDR shows persistent positive biases over most of the time period with a hint of somewhat larger bias during the boreal summer months (Figure 1d).

3.2. Validation of VIIRS Land AOT Retrievals With AERONET

Additional calibration/validation work was carried out to extend the preliminary evaluation of the VIIRS Land AOT reported in *Liu et al*. [2014]. With a much longer data record and quality assured AERONET data sets available, we compared the VIIRS AOT EDR and IP products to the AERONET Level 2.0 ground measurements.

The statistics of accuracy, precision, uncertainty, and correlation are presented in Figures 2a and 2b and also summarized in Table 1. A map of the 367 AERONET sites used in the analysis is shown in Figure 2c. As shown in Figure 2a, the sample sizes, accuracy, precision, uncertainty, and correlation coefficient in the Land AOT EDR versus AERONET are 29145, −0.0008, 0.116, 0.116, and 0.817, respectively. Although there are no maturity evaluation requirements for the IP products, the same set of statistical parameters are derived. The values for the Land AOT IP versus AERONET are 20269, 0.0415, 0.155, 0.160, and 0.741, respectively (see Table 1 and Figure 2b). Better performance of the land AOT EDR is expected because when IP AOT is aggregated to EDR AOT, the top 40% and bottom 20% of the available AOT IP retrievals within the 8×8 aggregation box are not included. This is done to exclude data artifacts associated with subpixel cloud contamination or cloud shadows.

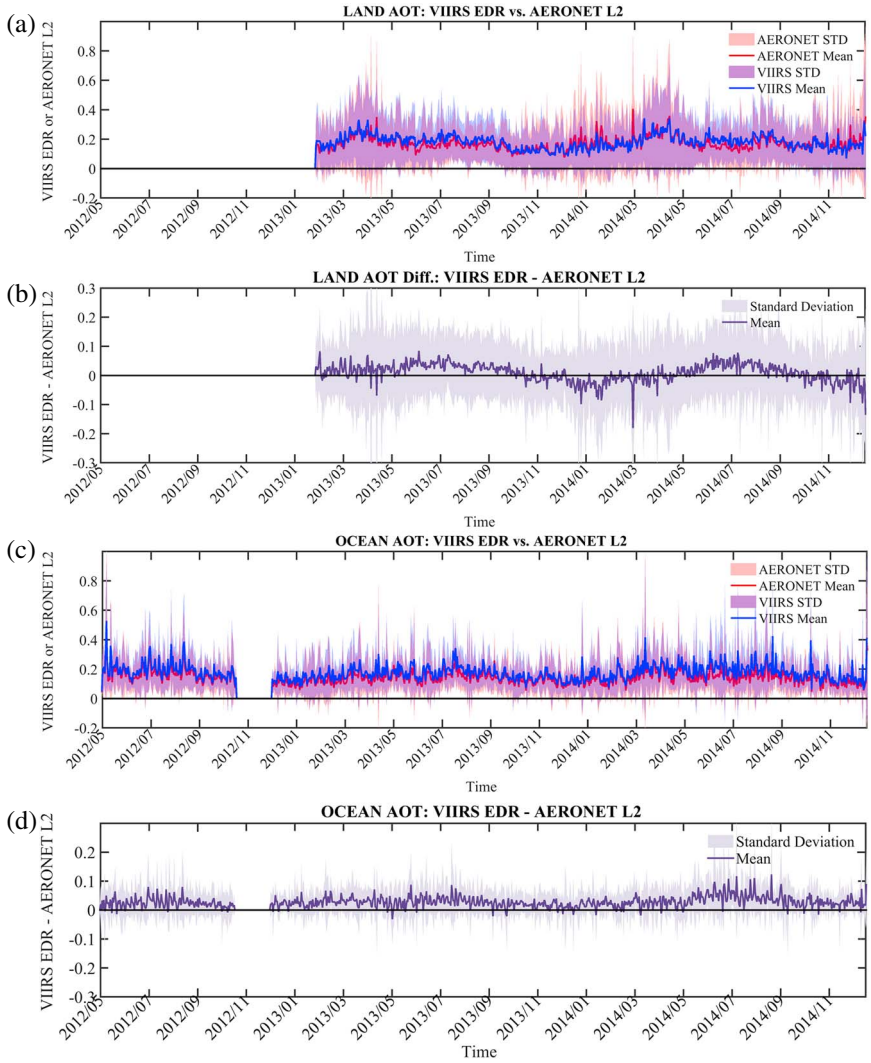

Figure 1. Time series of globally averaged VIIRS AOT EDR and AERONET L2.0 computed from the matchup data set (a) Land Daily AOT Means, (b) Land Daily AOT Mean Differences, (c) Ocean Daily AOT Mean, and (d) Ocean Daily AOT Mean Differences. Only collocated data are included in the global mean; therefore, the analysis is biased to AERONET station locations and to the times when both AERONET and VIIRS are reporting a high-quality observation or retrieval. In particular, the ocean time series is biased to coastal and island locations, which may not represent the open ocean well.

The regional characterization of the AOT difference between VIIRS and AERONET is shown in Figure 2c. Colors indicate the magnitude and sign of the bias. Spatially, the performance of VIIRS Land AOT EDR compared to AERONET varies with a clear regional dependency in the bias. In comparison to AERONET, VIIRS has a large negative bias over India and central Africa but a high bias over the Eastern U.S., the Island of Java, and at high-latitude regions in the northern hemisphere. Such regional dependence warrants more in-depth investigations of the algorithm performance in different regions of interest. More regional analysis will be discussed in section 3.6.

3.3. Validation of VIIRS Ocean AOT Retrievals With AERONET

The VIIRS aerosol algorithm over ocean is different from that over land [*Jackson et al.*, 2013]. Evaluation of the VIIRS aerosol retrievals over ocean was conducted by comparing AERONET measurements at coastal sites to the surrounding VIIRS retrievals but for ocean retrievals only. The locations of the 146 sites that contributed to the statistics are shown in Figure 3c. With much longer data availability and better quality assured AERONET data sets, we compared VIIRS Ocean AOT at both EDR and IP levels to AERONET L2.0 AOT. Statistical metrics of

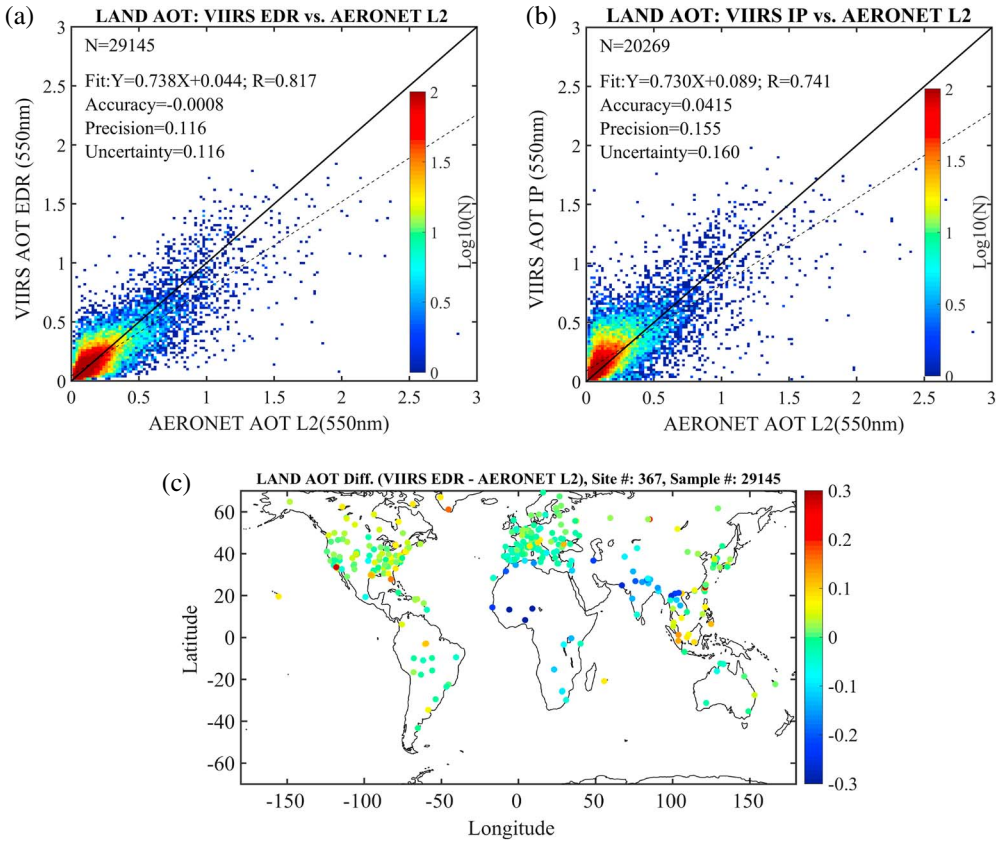

Figure 2. VIIRS Land AOT versus AERONET L2: (a) Density scatterplot of AOT EDR versus AERONET, (b) density scatterplot of AOT IP versus AERONET, and (c) mean AOT difference between VIIRS AOT EDR and AERONET at the contributing AERONET stations.

accuracy, precision, uncertainty, and correlation are shown in the scatterplots of Figure 3 and are also summarized in Table 1.

The overall performance of VIIRS Ocean AOT retrievals at both EDR and IP levels are shown in Figures 3a and 3b, respectively. As shown in Figure 3a, the sample sizes, accuracy, precision, uncertainty, and correlation coefficient in the Ocean AOT EDR versus AERONET are 17663, 0.0252, 0.060, 0.065, and 0.919, respectively. Over ocean the statistical metrics of IP and EDR AOTs are very similar. The same set of these statistical values from the Ocean AOT IP versus AERONET are 12107, 0.0273, 0.054, 0.061, and 0.926, respectively (see Table 1 and Figure 3b). The overall performance of VIIRS Ocean AOT retrievals is better than the land counterpart because over land, surface brightness and roughness vary with much more heterogeneity than over ocean, and thus, characterizing land surface at high spatial resolution is challenging and causing higher retrieval errors in land AOT retrievals.

Table 1. Summary of the Statistics From the VIIRS AOT 550 nm Versus AERONET L2.0 AOT 550 nm Scatterplots[a]

	Land AOT EDR	Land AOT IP	Ocean AOT EDR	Ocean AOT IP	Ocean AE EDR	Ocean AE IP
Sample size	29145	20269	17663	12107	7548	4388
Accuracy	−0.0008	0.0415	0.0252	0.0273	0.115	0.082
Precision	0.116	0.155	0.060	0.054	0.558	0.591
Uncertainty	0.116	0.160	0.065	0.061	0.570	0.597
Corr. coef.	0.817	0.741	0.919	0.926	0.676	0.679
Slope	0.738	0.730	0.967	0.958	0.457	0.429
Intercept	0.044	0.089	0.030	0.033	0.607	0.619

[a]Data periods: 23 January 2013 to 31 December 2014 for land and 02 May 2012 to 31 December 2014 for ocean. AERONET L2.0 data were acquired on 30 August 2015.

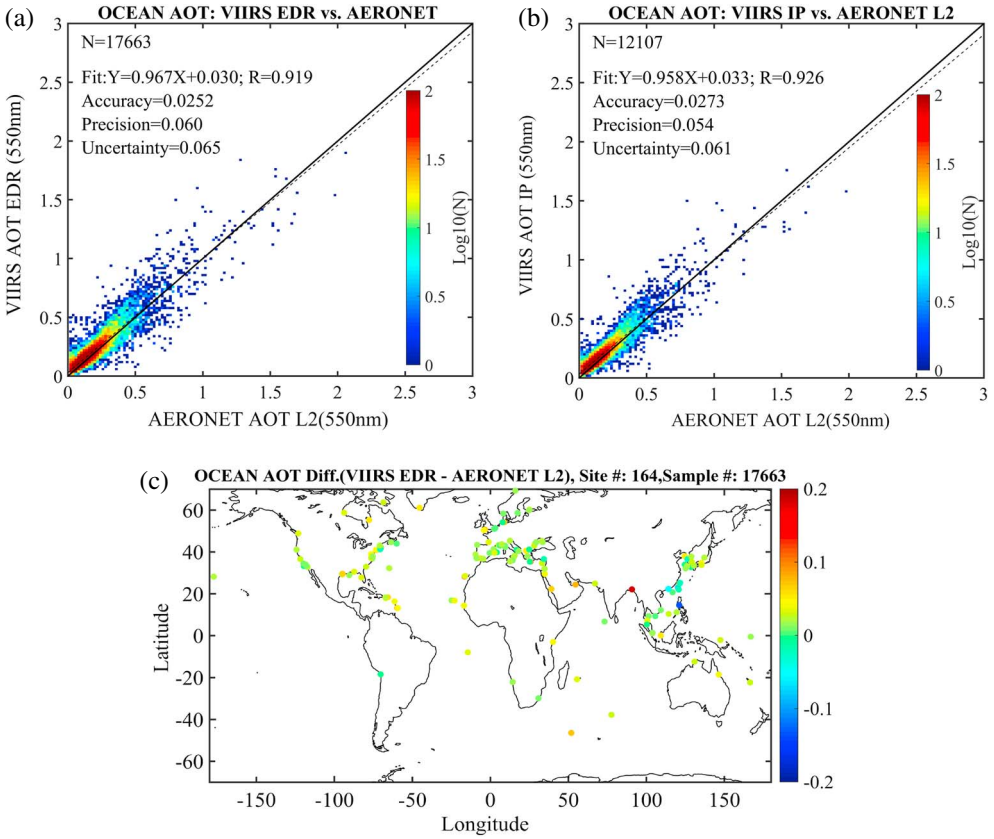

Figure 3. VIIRS Ocean AOT versus AERONET L2: (a) Density scatterplot of AOT EDR versus AERONET, (b) density scatterplot of AOT IP versus AERONET; and (c) mean AOT difference between VIIRS AOT EDR and AERONET at the contributing AERONET stations.

The regional characterization of the AOT difference between VIIRS and AERONET in Figure 3a is shown in the map of Figure 3c. In comparison to Figure 2c for the Land AOT EDR, the AOT biases between VIIRS Ocean AOT EDR and AERONET are small and have minimal regional differences. More regional analysis with selective regions of interests will be discussed in the section 3.6.

3.4. Validation of VIIRS Ocean AE Retrievals With AERONET

Although only the validation of the VIIRS AOT at 550 nm was discussed above, the VIIRS aerosol EDR products provide spectral AOT at 11 wavelengths from 412 nm to 2250 nm. From the spectral AOT values at two wavelengths (445 nm and 672 nm over land and 865 nm and 1610 nm over ocean), AE is calculated and provided to the users. In this analysis, only good quality AE retrievals were used. A good quality AE retrieval not only requires all quality assurance procedures by screening out unfavorable retrieval conditions (such as cloudy or snow pixels) but also requires the corresponding AOT retrieval at 550 nm to be greater than or equal to 0.15. This requirement is to avoid larger uncertainty in AE retrievals associated with low AOT because the spectral AOT errors are propagated to the AE retrievals when AE is calculated from two spectral AOTs [*Gobbi et al.*, 2007].

Figure 4 shows the comparison between the VIIRS Ocean AE (865 nm/1610 nm) EDR and AERONET. A map of the mean AE differences between VIIRS AE EDR and AERONET at 367 AERONET stations are shown in Figure 4 c. As shown in Figure 4a, the sample size, accuracy, precision, uncertainty, and correlation coefficient for the Ocean AE EDR versus AERONET are 7548, 0.115, 0.558, 0.570, and 0.676, respectively. Similarly, the sample size, accuracy, precision, uncertainty, and correlation coefficient in the Ocean AE IP versus AERONET are 4388, 0.082, 0.591, 0.597, and 0.679, respectively (see Table 1 and Figure 4b), providing essentially the same quality as the EDR, but with a much finer spatial resolution. The scatter shown in Figure 4a has a regional pattern, which is shown in the map of Figure 4c. Western U.S. coasts have positive AE biases but

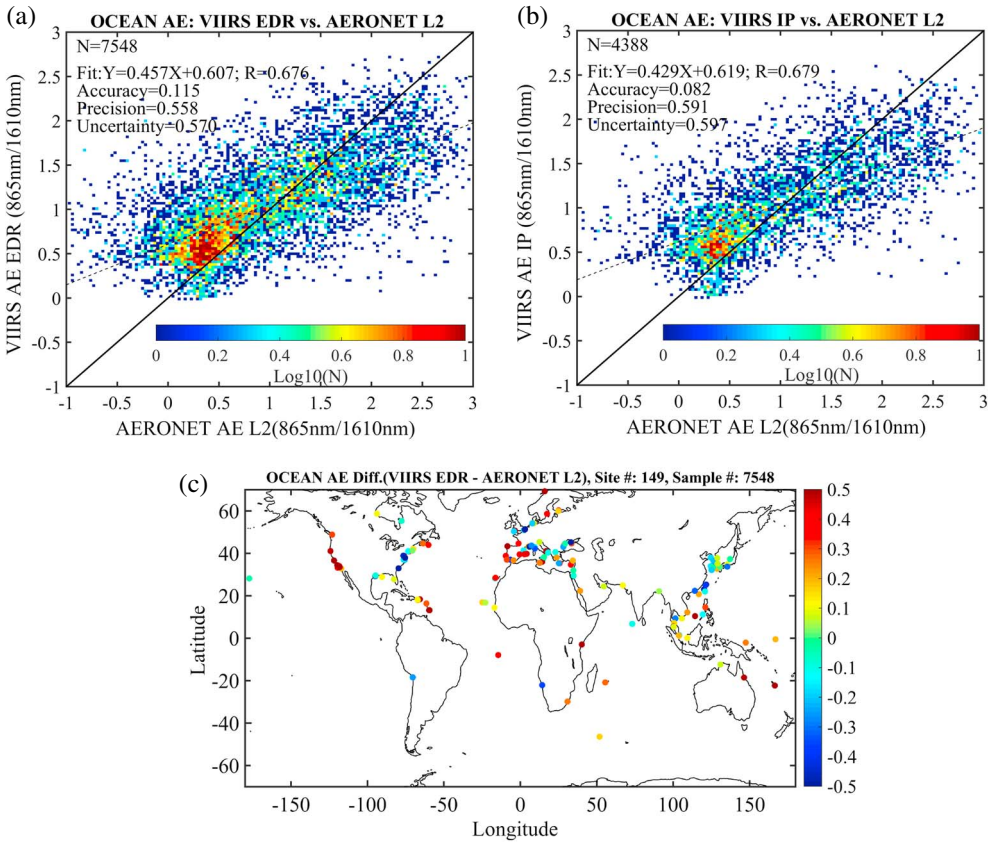

Figure 4. VIIRS Ocean AE versus AERONET L2: (a) Density scatterplot of AOT EDR versus AERONET, (b) density scatterplot of AOT IP versus AERONET, and (c) mean AE difference between VIIRS AE EDR and AERONET at the contributing AERONET stations.

Eastern U.S. coasts have negative AE biases. Analysis of AE retrievals over land is not being reported because there is no skill in the algorithm to derive the information. This is a known aerosol remote sensing problem and is widely reported in literature for MODIS, and the land AE is no longer reported in the MODIS Collection 6 Dark Target aerosol product [*Levy et al.*, 2013].

3.5. Spectral VIIRS AOT EDR Versus AERONET

As mentioned previously, the VIIRS EDR product reports spectral AOT at 11 wavelengths: 412 nm, 445 nm, 488 nm, 550 nm, 555 nm, 672 nm, 746 nm, 865 nm, 1240 nm, 1610 nm, and 2250 nm. Based on the available AERONET spectral AOT measurements (see section 2.3), we are able to assess the performance of the VIIRS AOT EDR at different selected wavelengths. Because of the much reduced data availability and large uncertainty in the AERONET data at wavelengths longer than 865 nm, most of which are extrapolated, we do not show the results for the VIIRS spectral AOT at wavelengths longer than 865 nm. The plots in Figure 5 provide an overall summary of the accuracy and precision for spectral AOT EDRs at wavelengths up to 865 nm. As shown in Figures 5a and 5b, for the VIIRS Land spectral AOT EDR, as the wavelength gets longer from 412 nm to 865 nm, the mean AOT bias (red line in Figure 5a) decreases from +0.014 to −0.006 and the precision (blue line in Figure 5b) decreases from 0.153 to 0.090. Similar for the VIIRS Ocean spectral AOT EDR, as the wavelength gets longer from 412 nm to 865 nm, the mean AOT bias (cyan line in Figure 5a) decreases from +0.0445 to +0.0056 and the mean standard deviation of the AOT bias (black line in Figure 5b) decreases from 0.080 to 0.045. In contrast to the VIIRS land AOT retrievals, the ocean AOT shows more positive biases but less retrieval uncertainty.

It is worthwhile to note, however, that although the mean bias and precision decrease with increasing wavelength, it does not mean the aerosol retrieval at higher wavelengths is more accurate than at lower wavelengths. As shown in Figure 5c, the absolute magnitude of the spectral AOT also decreases with

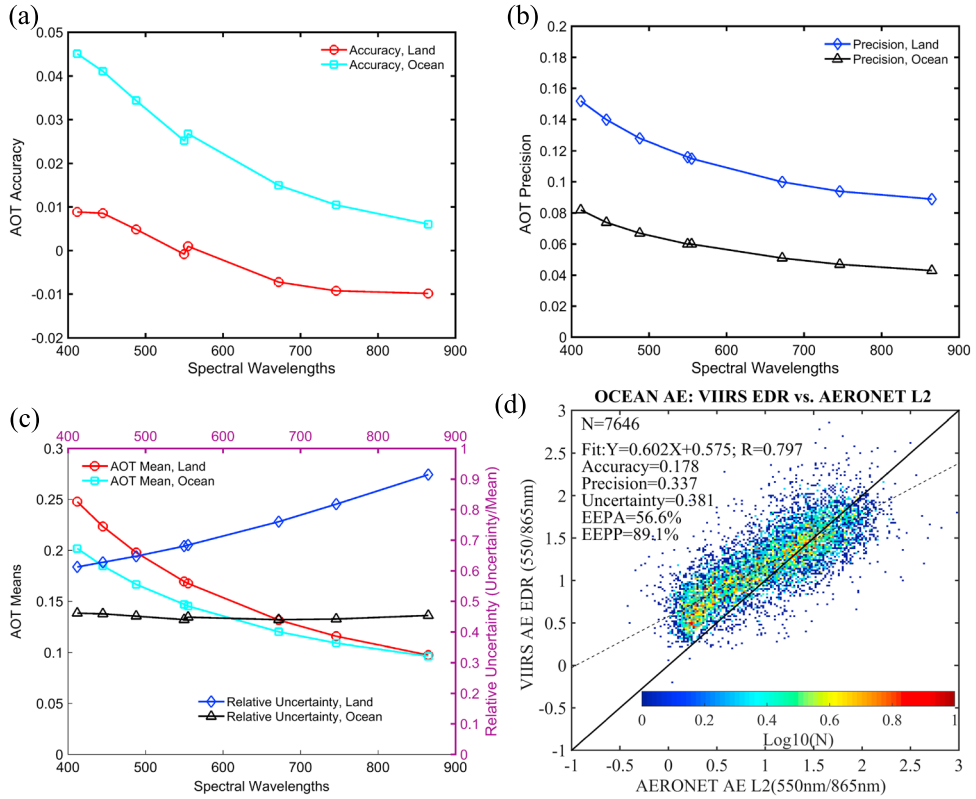

Figure 5. (a) Accuracy for VIIRS spectral AOT retrievals at eight wavelengths in visible and near infrared, over land and ocean respectively. (b) Precision for VIIRS spectral AOT retrievals at eight wavelengths in visible and near infrared, over land and ocean respectively. (c) AOT means and relative uncertainty at the same wavelengths, over land and ocean respectively. (d) VIIRS versus AERONET Angström Exponent calculated from the spectral AOT at 550 nm and 865 nm.

wavelengths, but the relative uncertainty, defined as the root mean square error of AOT biases divided by the AOT mean, actually increases with wavelengths.

The correlation between the VIIRS and AERONET spectral AOT over land also decreases from 0.846 to 0.506 as the wavelength gets longer from 412 nm to 865 nm. For the VIIRS Ocean spectral AOT EDR, however, as the wavelength gets longer from 412 nm to 865 nm, the correlation coefficient stays high from 0.911 to 0.913. Such dramatic differences in the correlation between the land and ocean retrievals demonstrate that the overall uncertainty in the VIIRS Land AOT retrievals is higher than its ocean counterpart. This also warrants more in-depth investigations with land aerosol model stratifications so that we can have a better understanding of the performance of each land aerosol model for retrieving AOT at various spectral wavelengths.

While the standard VIIRS operational aerosol product only offers an AE over ocean calculated from the 865 nm and 1610 nm wavelengths, AE can be calculated from the AOTs at any two separate wavelengths. An AE calculated from the wavelength pair of 550 nm and 865 nm represents AOT spectral dependence through the visible and near-infrared bands, an important spectral range for a variety of applications. It also happens to be one of the wavelength pairs used for calculating AE in the MODIS aerosol product. Figure 5d shows the density-scatterplot of the VIIRS Ocean AE versus AERONET AE that is calculated from the AOTs at 550 nm and 865 nm wavelengths. In comparison to the VIIRS operational ocean AE product in Figure 4a, this AE seems to have relatively higher mean biases (0.178 versus 0.115) but much less uncertainty (0.381 versus 0.570). The correlation coefficient of the two AE pairs also increased from 0.676 to 0.797. This indicates that the validation of AE or spectral AOT depends on the wavelengths chosen.

3.6. Regional and Seasonal Variability of VIIRS AOT and AE EDR

Figures 2c, 3c, and 4c have shown regional differences in the bias between VIIRS and AERONET AOT or AE. A more detailed analysis was conducted by dividing the global retrievals into several dust or biomass burning

regions so that both regional and seasonal variability of the VIIRS versus AERONET difference with different aerosol species can be evaluated at the same time. Analysis is performed for nine regions of interest (ROI) over land (Western U.S., Eastern U.S., India, East Asia, Canada, South America, Europe, south Africa, and central Africa) and four regions over ocean (North Tropical Atlantic, South Tropical Atlantic, North Indian Ocean, and Northwestern Pacific). The definition of these ROIs can be seen in Figure 6a. For each region, the daily mean deviations of the VIIRS AOT or AE EDR retrievals from the paired AERONET measurements were first calculated and a 30 day running mean was applied to the daily data sets for better observations of seasonal variability in the time series.

The smoothed daily time series for the nine land ROIs can be seen as Figure 6b. The most significant variability is found over India with strong negative biases in the VIIRS Land AOT retrievals during boreal spring seasons when the most intensive agricultural biomass burning activities occur during local harvesting season. Other areas with biomass burning activity show similar negative bias (central Africa and south Africa). In contrast, large positive biases occur during boreal spring to boreal fall but never in boreal winter. Such regionally dependent seasonal variability in the VIIRS Land AOT retrievals provides the evidence that the VIIRS land aerosol algorithm can be improved by using dynamic surface reflectance ratios instead of global constants [*Liu et al*., 2014]. Also, further evaluation of the biomass burning smoke AOT retrieval and the algorithm's choice of aerosol model for smoke events seem warranted.

On the other hand, the VIIRS Ocean AOT EDR shows an overall positive bias (Figure 6c). North Tropical Atlantic where African dust outbreaks frequently happen seems to drive the global statistics more significantly than the other regions. North Tropical Atlantic has three positive peaks, all during boreal summer times, when African dust outbreaks are usually prevalent [*Huang et al*., 2010]. In contrast to the Northwestern Pacific where more negative AE biases indicated that too many coarse particles were detected in the algorithm, more positive AE biases in the VIIRS AE EDR occurred over the North Tropical Atlantic, as observed in Figure 6d. The AE overestimation indicates too many fine particles detected by the retrieval algorithm when coarse African dust particles were present, in line with the high bias of the fine mode fraction we observed when compared this parameter with those from MODIS and MISR. This is intriguing because fine particles have stronger back scattering than larger particles, so theoretically more counting of fine particles should lead to underestimation of AOT. But this is not seemingly the case for North Tropical Atlantic where both positive AE and AOT errors were found. Therefore, solely attributing the positive AOT error to too high of a fine mode fraction in the algorithm may not be adequate. For the case over North Tropical Atlantic during the dust laden boreal summer months, it is also worthwhile to explore whether the positive AOT biases are a consequence of modeling the spheroid dust particles as spherical using the Mie theory. *Yang et al*. [2007] showed that the phase functions of spherical particles are much larger than its spheroidal counterparts in forward directions (scattering angles $< 5°$) and backward directions ($>150°$), but much less at scattering angles between 90° and 150°. In our matched up data sets, however, most of the scattering angles over North Tropical Atlantic were between 90° and 150°, implying that the assumption of spherical dust particles in the coarse model could result in AOT overestimation because of the relatively lower phase function of spherical particles. And consequently, the AOT overestimation attributable to substituting spherical particles for spheroidal particles is more significant for shorter wavelengths than longer wavelengths [*Yang et al*., 2007], leading to positive AE biases over the dust prevalent North Tropical Atlantic.

3.7. Evaluation of Land Aerosol Model Selection in the VIIRS Land AOT

The dynamic selection of the land aerosol models is another potential factor for data uncertainty in the VIIRS Land AOT retrievals. As described with more details in *Jackson et al*. [2013], there are five land aerosol models in the land aerosol algorithm: Dust, Smoke High Absorption, Smoke Low Absorption, Urban Clean, and Urban Polluted. The models include size distributions and optical properties of the aerosols with some of the parameters varying with magnitude of the AOT [*Remer and Kaufman*, 1998].

To evaluate the performance of each land aerosol model, we used the VIIRS IP versus AERONET matchup data sets. For each VIIRS IP versus AERONET matchup within the domain and time period, the most often selected land aerosol model was identified. Out of all the matchup samples, the fraction of each land aerosol model for the VIIRS IP-AERONET matchup is shown in Figure 7a. The Dust model is selected most often (43% of the time) followed by the Urban Clean model (32%), Smoke Low Absorption (12%), Urban Polluted (8%), and Smoke High Absorption (5%). Figure 7c further illustrates the regional distribution of the most often selected land

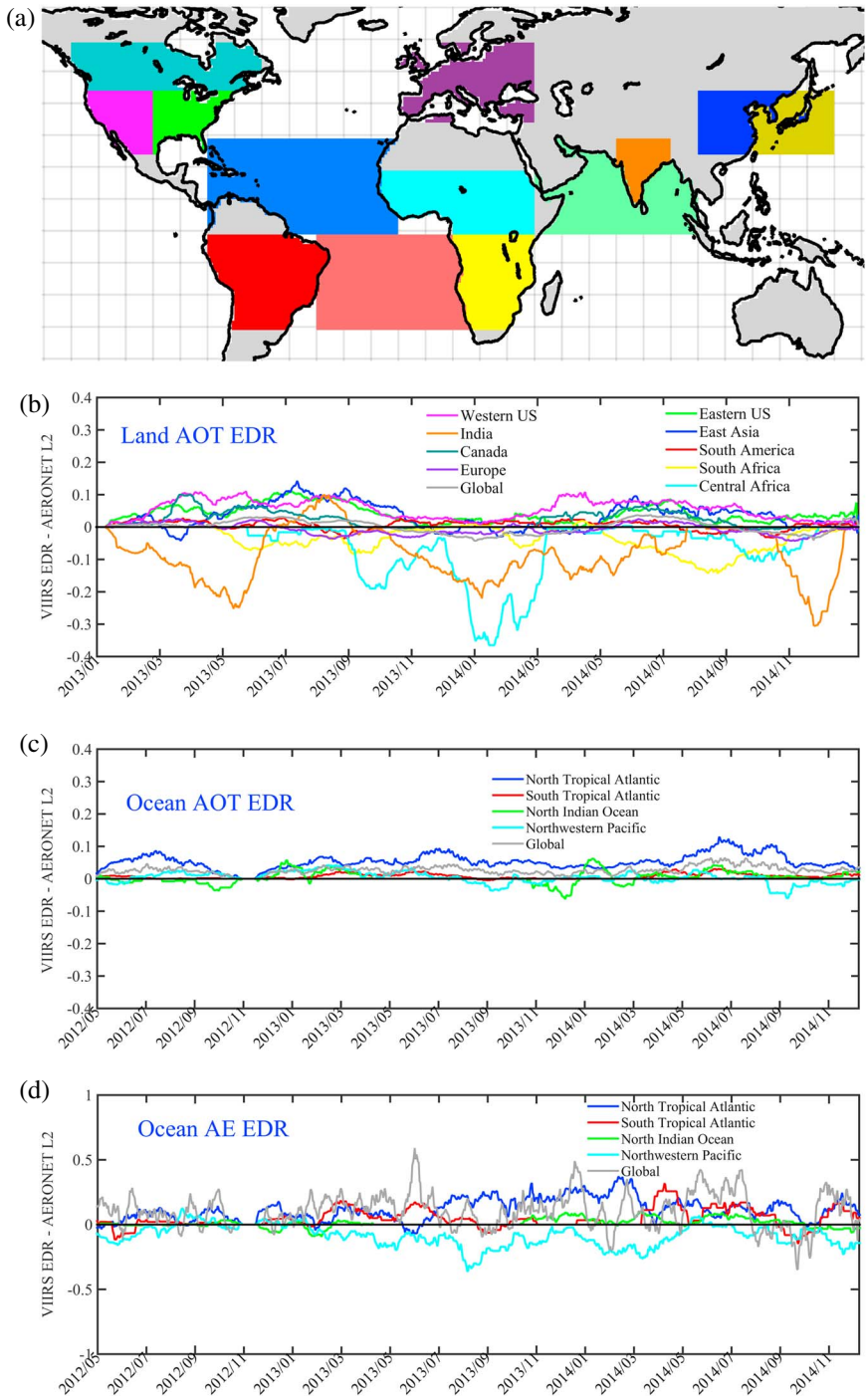

Figure 6. Seasonal variability of VIIRS AOT and AE EDR versus AERONET: (a) Maps of ROIs, (b) Land AOT, (c) Ocean AOT, and (d) Ocean AE 865 nm/1610 nm.

aerosol model at each AERONET site. For example, the Dust model is the most often selected model over the Sahara, Western U.S., Western Europe, and Australia, etc. Sometimes, it is also selected over the Amazon where dust is not common, indicating a potential aerosol model selection issue in the algorithm. Because coarse dust particles are less scattering than fine smoke particles, modeling smoke with dust models leads to positive AOT bias. However, the significance of such influence from the mismatched aerosol model over Amazon is still unclear because Figure 6b did not show significant positive bias over South America. The

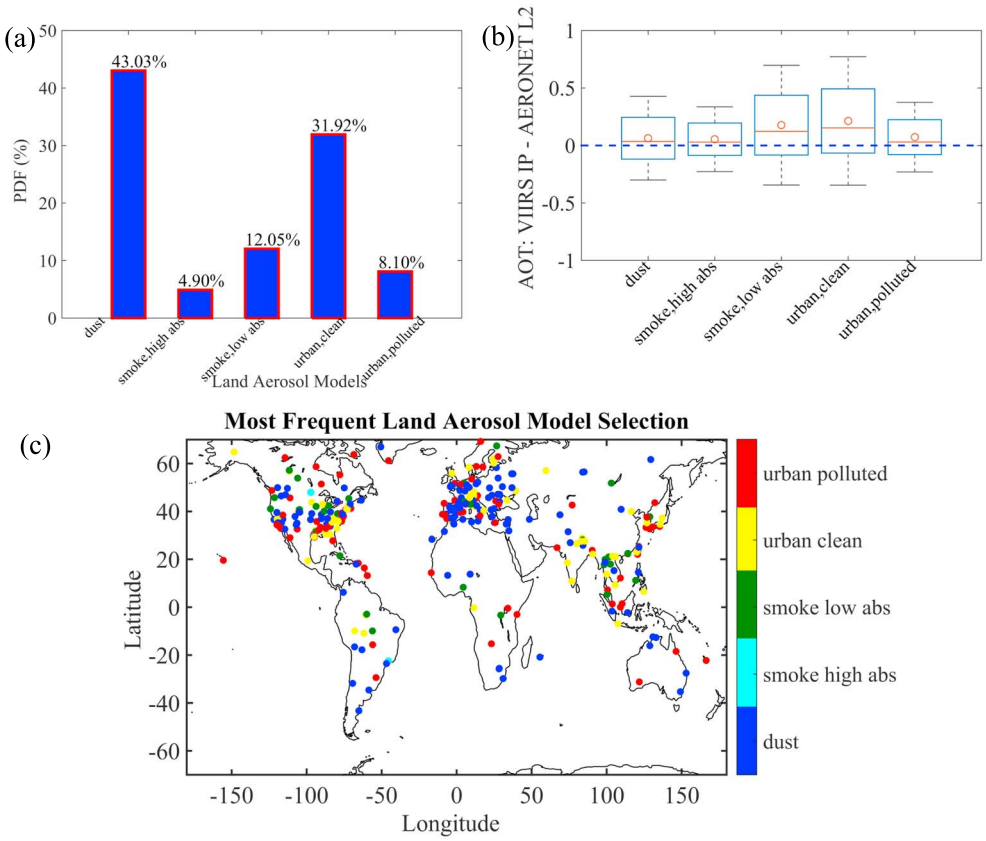

Figure 7. Land aerosol model selection in the AOT matchups of VIIRS IP and AERONET L2: (a) probability distribution function of each model selection; (b) AOT differences for each model. The means, medians, and 1 standard deviation intervals of the VIIRS IP-AERONET differences are the red circles, the red center lines, and blue boxes in the vertical, respectively. The black whiskers are the 2 standard deviation intervals; (c) most frequently selected model at each matchup AERONET site.

mean and standard deviation of the retrieval biases for each model are compared in Figure 7b. The Urban Clean model and the Smoke Low Absorption model seem to cause larger positive biases and larger data uncertainty in comparison to the other three models.

3.8. Relation of VIIRS Land AOT Biases to Aerosol Particle Size

To see whether the Land AOT biases are related to aerosol particle sizes, we plotted the differences between VIIRS and AERONET Land AOT against AERONET measured AE and then linked the results to the corresponding land model selections. Figure 8 shows the mean and standard deviation of the VIIRS versus AERONET AOT differences in 50 bins of AERONET AE. Systematic changes in the land AOT biases as a function of AE are observed. These systematic changes are described as the best linear fit of AERONET AE to the mean biases (EA) and the best linear fit of AERONET AE to the 1 standard deviation of the biases (EP). The expected error (EE) is calculated as a combination of EA and EP (see Figure 8). EA of land AOT as a function of AERONET AE changes from negative to positive as AE increases, indicating more positive biases for fine particles. EP as the indicator of the data uncertainty in land AOT, however, decreased as AERONET AE increased, showing less data uncertainty for land AOT retrievals for fine particles. The matchup samples were almost evenly distributed when the AERONET AE is between 1 and 2, where biases were generally near zero and standard deviations remained constant across the AE bins. Thus, the extreme AE bins, at the low and high ends of the distribution, influence most of the systematic variations captured by the linear fits.

The land model selection in each AERONET AE bin aligned with expectations that the coarse mode model (dust model) would be associated with small AE and fine mode model (the aggregation of the four other land aerosol models) with large AE. Indeed, the dust model fraction is ~0.70 when the AERONET AE

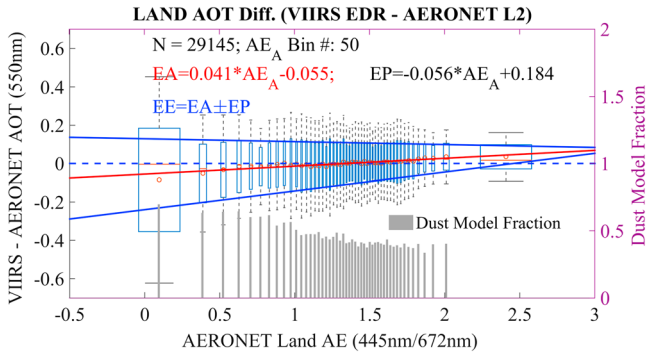

Figure 8. Sensitivity of the difference between VIIRS EDR and AERONET AOT Land AOT to the AERONET AE. The red line is the Expected Accuracy (EA), the best linear fit to the mean biases (red circles). The expected precision (EP) is estimated as the best linear fit to the 1 standard deviation of the biases (the vertical top-bottom blue intervals). The two blue lines are the expected error (EE) calculated based on EA and EP. The gray vertical lines are the fraction in each AE bin that the dust model is selected and is quantified with the right-hand side axis and labels.

indicates coarse particles, and this fraction reduces to ~0.30 as AERONET AE increases becoming dominated with more fine particles.

3.9. Relation of VIIRS Land AOT Biases to Ground Vegetation Conditions

As extensively discussed in *Liu et al.* [2014], the biases in the VIIRS Land AOT retrievals are potentially related to surface conditions such as surface brightness and vegetation coverage. In this study, this investigation is extended to the possible influence of surface reflectance assumptions on retrieval uncertainty by using the extended data period to identify the sensitivity of the retrieval biases to vegetation indices that describe surface conditions. Figure 9 shows the mean and standard deviation of the VIIRS versus AERONET biases over 50 bins of a near-infrared (NIR)-based normalized difference vegetation index:

$$\mathrm{NDVI_{NIR}} = (\mathrm{M8\text{-}M5})/(\mathrm{M8} + \mathrm{M5}) \quad (1)$$

where M5 is the 672 nm red band and M8 is the 1240 nm NIR band reflectances. This NDVI features a reference wavelength in red and a measurement wavelength in NIR, and thus is also called $\mathrm{NDVI_{1240\ nm}}$ in some literature [*Huang et al.*, 2009] for vegetation water content monitoring purposes. In Figure 9, the mean and standard deviation of the biases are strongly related to ground vegetation growth and vegetation water content that is better presented with this vegetation index. The mean AOT bias changes systematically from −0.2 to +0.02, and the standard deviation of the biases decreases significantly from 0.5 to 0.07 as this $\mathrm{NDVI_{1240\ nm}}$ increases from ~0.1 to 0.7. Figure 9 implies that the relationship between $\mathrm{NDVI_{NIR}}$ and surface reflectance ratios can help build a more dynamic surface reflectance ratio database as a function of ground vegetation conditions. This should aid in reducing data product uncertainty in the land AOT retrievals and improve the overall performance of the VIIRS land AOT product. The results are consistent with the *Liu et al.* [2014] findings that at least part of the systematic biases are attributable to the dependence of spectral surface reflectance ratios on vegetation coverage because the current VIIRS algorithm prescribes globally constant spectral surface reflectance ratios without accounting for the variation of surface type [*Liu et al.*, 2014]. The prescribed spectral surface reflectance ratios are optimally matched by the spectral surface reflectance ratios calculated in the land aerosol models after correction for aerosol and other atmospheric effects with optimally selected aerosol models and aerosol loadings [*Vermote and Kotchenova*, 2008]. To improve the VIIRS land AOT performance, some exploratory work was conducted in *Liu et al.* [2014] by introducing ground vegetation condition dependence in the spectral surface reflectance ratios.

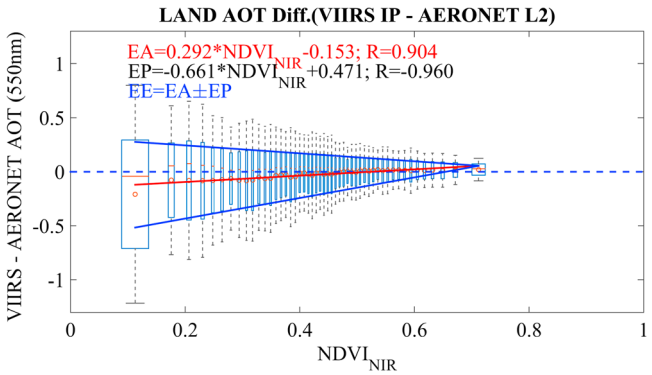

Figure 9. Dependence of the difference between VIIRS best quality IP and AERONET Land AOT to a NIR-based NDVI, $\mathrm{NDVI_{NIR}}$ = (M8-M5)/(M8 + M5), with M5 at 672 nm and M8 at 1240 nm.

4. Expected Error Estimation

Expected error (EE) is a validation metric often used when satellite aerosol retrievals are validated against

ground measurements, but EE has no universally accepted definition, and thus varies wildly in the literature. The EE for the MODIS aerosol products was mostly estimated based on the assumption of a Gaussian distribution of the biases from the MODIS retrievals to AERONET [e.g., *Levy et al*., 2010; *Remer et al*., 2005; *Sayer et al*., 2013; *Hsu et al*., 2013]. With such an assumption, EE is the envelope that encompasses 68% of the samples with least bias. In the literature, the EE values for the MODIS Dark Target aerosol product were defined as the difference between retrieval product and AERONET, as a function of the AERONET measurements. The EE values for the Collection 6 MODIS Deep Blue aerosol product are defined as the product-AERONET differences as a function of the satellite retrievals, in order to produce a calculated data bias as part of the output in the aerosol product. Moreover, the geometric air mass factor (AMF, the sum of the cosines of the solar and sensor zenith angles) was also used in the EE estimation equation [*Sayer et al*., 2013]. To define the EE for the VIIRS aerosol products, namely, Land AOT, Ocean AOT, and Ocean AE, we explored the following four approaches: (1) EE based on EA and EP that are functions of the AERONET measurements, where EA is the expected accuracy derived from mean biases and EP is the expected precision derived from 1 standard deviation of biases (i.e., Figure 10a), (2) EE based on EA and EP that are functions of the VIIRS observations (i.e., Figure 10b), (3) EE estimated by the 68% sample percentile method similarly as in *Sayer et al*. [2013] with the use of AMF (i.e., Figure 10c), and (4) EE estimated as in (3) but without taking AMF into account (i.e., Figure 10d). Based on these approaches, Figures 10 and 11 present the EE estimation results for the VIIRS land AOT and ocean AOT, respectively. All the EE estimation equations and the associated statistical parameters are summarized in Table 2 for comparison and references.

In order to estimate EE, Figure 10a first demonstrates how the VIIRS versus AERONET deviation varies with AOT loading in 50 AERONET AOT bins. All 29145 AOT matchup samples were divided into 50 AERONET AOT bins with equal sample sizes, and then mean, median, 1 standard deviation, and 2 standard deviations of the samples were calculated in each AERONET AOT bin. There are strong indications of positive biases in the VIIRS Land AOT at the lower bound of the AERONET AOT (<0.2), but negative biases at the higher bound of the AERONET AOT (>0.2). As a function of AERONET AOT, EA (red line) is estimated as the best linear fit to the mean biases (red circles): $-0.238\times\tau_A+0.040$, and EP is estimated as the best linear fit to the 1 standard deviation of the biases represented by the blue boxes: $0.232\times\tau_A+0.050$. The EE for the VIIRS Land AOT is then calculated as EA ± EP (two blue lines): $(-0.470\times\tau_A-0.010,\ -0.0058\times\tau_A+0.090]$, with 78.24% of samples falling into this range. Similarly, same as in Figure 10a, Figure 10b shows the EE estimation as a function of the VIIRS AOT observations: $(-0.249\times\tau_V-0.054,\ 0.519\times\tau_V+0.010)$, with $EA=0.135\times\tau_V-0.022$, $EP=0.384\times\tau_V+0.032$ and 80.01% of the samples falling within the EE range. Following the same approach as in *Sayer et al*. [2013] by including AMF in the EE calculation, the EE of the VIIRS land AOT can be calculated as $(0.54\times\tau_V+0.030)/AMF$, which seems to be slightly better than the same EE estimation equation for the MODIS Collection 6 Deep Blue land aerosol product: $(0.56\times\tau_M+0.086)/AMF$, where τ_M is the MODIS Deep Blue AOT. Figure 10d is the same as Figure 10c except that the EE estimation did not take AMF into account: $0.34\times\tau_V+0.022$. Although AMF was not considered, the correlation of the 68% percentile line stays very significant with essentially the same correlation coefficient or *p*-value, indicating that taking AMF into account does not seem to impact the EE estimation significantly.

Similarly, Figure 11 showed the EE estimation for the VIIRS Ocean AOT. As a function of AERONET AOT in Figure 11a, $EA=-0.022\times\tau_A+0.029$, $EP=0.216\times\tau_A+0.019$, and $EE=(-0.238\times\tau_A+0.010,\ 0.194\times\tau_A+0.048)$ with 75.61% samples inclusive. Although the magnitudes were small, these matchups, mostly coastal regions, seem to have positive biases, consistent with the time series in Figure 1d. In agreement to Figures 1d and 3c, the VIIRS Ocean AOT seems to have small positive biases of approximately 0.02–0.03 at almost every AOT bin as shown in Figures 3a and 3b, except for the last AERONET AOT bin where the mean AOT is about 0.8. Although it is difficult to see in the plot, we note that there is a high positive bias of ~0.07 when the AERONET AOT is as low as 0.01. When the VIIRS minus AERONET AOD differences are plotted as a function of the VIIRS Ocean AOT in Figure 11b, $EA=0.130\times\tau_V+0.0028$, $EP=0.202\times\tau_V+0.013$, and $EE=(-0.071\times\tau_V-0.010,\ 0.332\times\tau_V+0.016)$ with 76.99% samples inclusive. With AMF, Figure 11c shows the 68th percentile $EE=(0.36\times\tau_V+0.012)/AMF$, and without AMF, Figure 11d shows $0.25\times\tau_V+0.009$ with essentially the same correlation coefficient as in Figure 11c. Comparing Figure 11 to Figure 10, the data uncertainty of the VIIRS Ocean AOT are only about half of that for the VIIRS Land AOT, presenting a much better performance of the VIIRS ocean aerosol algorithm than its land counterpart.

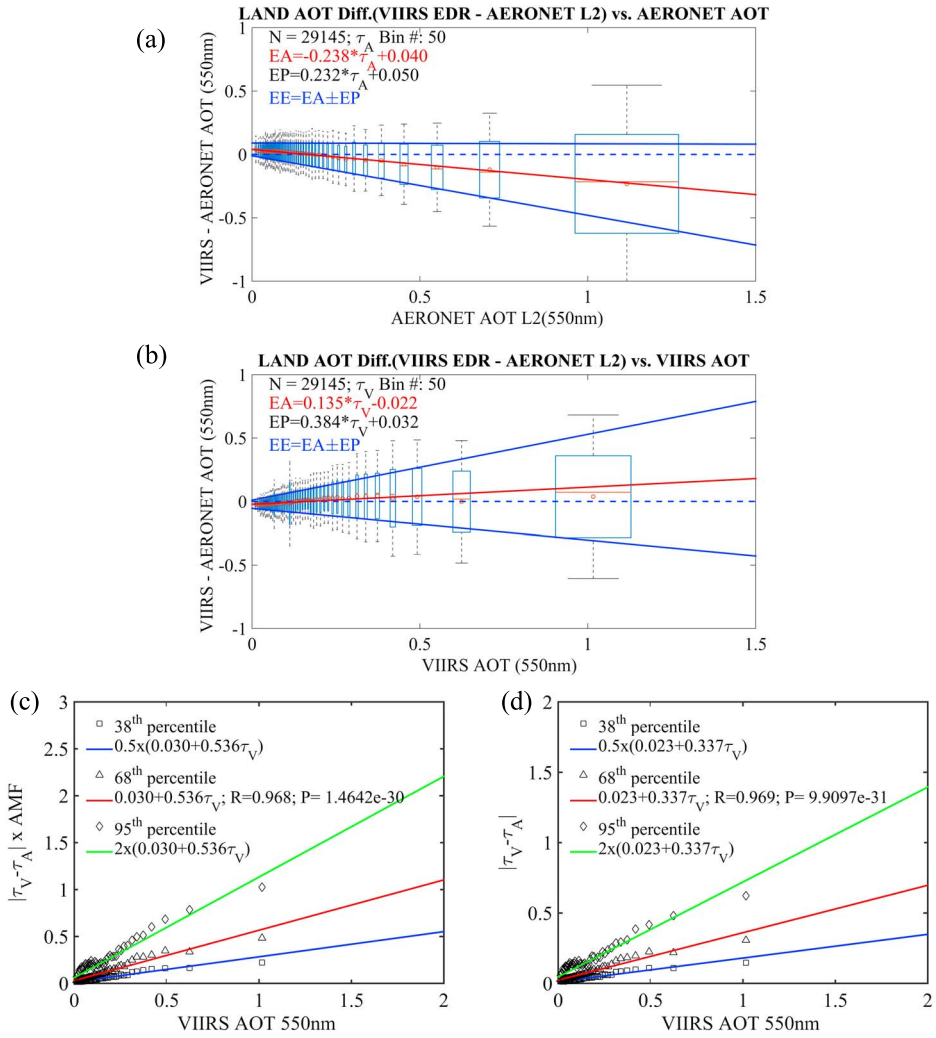

Figure 10. VIIRS Land AOT versus AERONET L2: (a) distribution of the AOT difference between VIIRS AOT EDR and AERONET plotted against AERONET AOT (the means, medians, and 1 standard deviation intervals of the VIIRS-AERONET differences are the red circles, the red center lines, and blue boxes in the vertical, respectively). The black whiskers are the 2 standard deviation intervals. The red line is the expected accuracy (EA), which is the best linear fit to the mean biases (red circles). The expected precision (EP) is estimated as the best linear fit to the 1 standard deviation of the biases (the tops or bottoms of the blue boxes). The two blue lines are the expected error (EE) calculated based on EA and EP. (b) Distribution of the AOT difference between VIIRS AOT EDR and AERONET plotted against VIIRS AOT. All the symbols and legends are the same as in Figure 10a. (c) The 38th (squares), 68th (triangles), and 95th (diamonds) sample percentiles of the AOT difference between VIIRS AOT EDR and AERONET as a function of VIIRS AOT, scaled by geometric air mass factor (AMF). The red line is the best linear fit of the 68th percentiles, the blue line half this linear fit, and the green line twice this linear fit. (d) Same as Figure 10c but without being scaled by geometric AMF, with the same symbols and legends as in Figure 10c.

As seen in the EA and EE estimation lines in Figures 10a and 10b and Figures 11a and 11b, because of the trending in the EA estimation, the distributions of the biases are not following ideal Gaussian distributions, which results in the asymmetrical EE ranges.

Following the same procedure to estimate EE for the VIIRS Ocean AE introduces complications. Figure 12a demonstrates the changing tendency of the VIIRS Ocean AE EDR's deviation from AERONET as a function of the AERONET AE. Consistent with Figures 4a and 4b, Figure 12a clearly illustrates strong positive biases in the VIIRS AE for coarse particles (low AERONET AE) but negative biases for fine particles (high AERONET AE): $EA = -0.536 \times AE_A + 0.603$ ($R = 0.962$), but EP is equal to a constant of 0.359, not showing any dependence on AERONET AE. In other words the retrieval uncertainty of the VIIRS Ocean AE EDR shown in Figure 12a does not seem to be sensitive to aerosol particle size. If the AE differences are plotted against VIIRS AE instead of

Table 2. Expected Errors in Reference to the AERONET Measurements and the VIIRS Observations, Respectively[a]

Ref.	Target	Estimation	R		*P* Value
LAND AOT (23 January 2013 to 31 December 2014)					
AERONET	EA	$-0.238\times\tau_A+0.040$	−0.986		2.48e-38
	EP	$0.232\times\tau_A+0.050$	0.984		4.20e-37
	EE (EA ± EP)	$(-0.470\times\tau_A-0.010,\ -0.0058\times\tau_A+0.090)$		78.2%*	
VIIRS	EA	$0.135\times\tau_V-0.022$	0.782		3.25e-11
	EP	$0.384\times\tau_V+0.032$	0.943		4.39e-24
	EE (EA ± EP)	$(-0.249\times\tau_V-0.054,\ 0.519\times\tau_V+0.010)$		80.0%*	
	EE (68% method)	No AMF $0.34\times\tau_V+0.023$	0.969		9.91e-31
		AMF $(0.54\times\tau_V+0.030)$/AMF	0.968		1.46e-30
OCEAN AOT (02 May 2012 to 31 December 2014, excluding 15 October 2012 to 27 November 2012)					
AERONET	EA	$-0.022\times\tau_A+0.029$	−0.394		0.0046
	EP	$0.216\times\tau_A+0.019$	0.951		4.62e-26
	EE (EA ± EP)	$[-0.238\times\tau_A+0.010,\ 0.194\times\tau_A+0.048]$		75.6%*	
VIIRS	EA	$0.130\times\tau_V+0.0028$	0.962		9.96e-29
	EP	$0.202\times\tau_V+0.013$	0.988		2.06e-40
	EE (EA ± EP)	$(-0.071\times\tau_V-0.010,\ 0.332\times\tau_V+0.016)$		77.0%*	
	EE (68% method)	No AMF $0.25\times\tau_V+0.009$	0.992		8.27e-45
		AMF $(0.36\times\tau_V+0.012)$/AMF	0.991		5.20e-44
OCEAN AE (02 May 2012 to 31 December 2014, excluding 15 October 2012 to 27 November 2012)					
AERONET	EA	$-0.536\times AE_A+0.603$	−0.962		7.51e-29
		$-0.253\times\log(\tau_A)$-0.273	−0.872		2.93e-15
	EP	0. 359	N/A		N/A
		$-0.150\times\log(\tau_A)+0.293$	−0.846		1.39e-13
	EE (EA ± EP)	$(-0.536\times AE_A+0.244,\ -0.536\times AE_A+0.962)$		69.1%*	
		$(-0.103\times\log(\tau_A)-0.566,\ -0.403\times\log(\tau_A)+0.020)$		69.8%*	
VIIRS	EA	$-0.024\times AE_V+0.135$	0.110		0.448
		$-0.164\times\log(\tau_V)-0.112$	−0.626		1.15e-06
	EP	0. 541	N/A		N/A
		$-0.221\times\log(\tau_V)+0.234$	−0.872		1.59e-16
	EE (EA ± EP)	$(-0.024\times AE_V-0.406,\ -0.024\times AE_V+0.676)$		71.3%*	
		$(0.057\times\log(\tau_V)-0.346,\ -0.385\times\log(\tau_V)+0.122)$		70.2%*	

[a]EA: expected accuracy, EP: expected precision, EE: expected error, AMF: air mass fraction, τ_A: AERONET AOT, τ_V: VIIRS AOT. The values in asterisks are the sample percentiles falling in the corresponding EE ranges.

AERONET AE (Figure 12b), the correlation of $EA=-0.024\times AE_V+0.135$ breaks down ($R=0.110$) and EP becomes approximately a constant value of 0.541.

On the other hand, however, if the AE difference values are plotted against AOT (or the logarithm of AOT) instead of AE, dependencies emerge and deepen. In Figure 13a EE is estimated as a function of AERONET AOT: $EA=-0.253\times\log(\tau_A)-0.273$, $EP=-0.150\times\log(\tau_A)+0.293$, and $EE=(-0.103\times\log(\tau_A)-0.566,\ -0.403\times\log(\tau_A)+0.020)$. In Figure 13b EE is estimated as a function of VIIRS AOT: $EA=-0.164\times\log(\tau_V)-0.112$, $EP=-0.221\times\log(\tau_V)+0.234$, and $EE=(0.057\times\log(\tau_V)-0.346,\ -0.385\times\log(\tau_V)+0.122)$.

Figures 13a and 13b show that there are specific AOT ranges where AE can be better defined for quality assurance. For example, in Figure 13a, as the AERONET AOT gets higher, the VIIRS Ocean AE EDR starts with a positive bias when AOT is less than 0.15, followed by reduced positive biases when AOT is between 0.15 and 0.20. After that, the mean bias gradually becomes negative as the AOT gets higher while the mean standard deviation of the bias becomes narrower. The current VIIRS AE algorithm degrades AE retrievals when AOT is lower than 0.15. Figure 13 further confirms that an AOT threshold value between 0.15 and 0.20 is very necessary in providing quality assured AE product with much reduced biases.

5. Discussions and Conclusions

To date, the VIIRS sensor has provided four years of high-quality daily global aerosol data. In this work, the VIIRS high-quality AOT EDR at 550 nm over both land and ocean, and the high-quality AE EDR over ocean, are validated against the Level 2.0 AERONET ground measurements. The validation period over land is 23 January 2013 to 31 December 2014, and the validation period over ocean is 2 May 2012 to 31 December

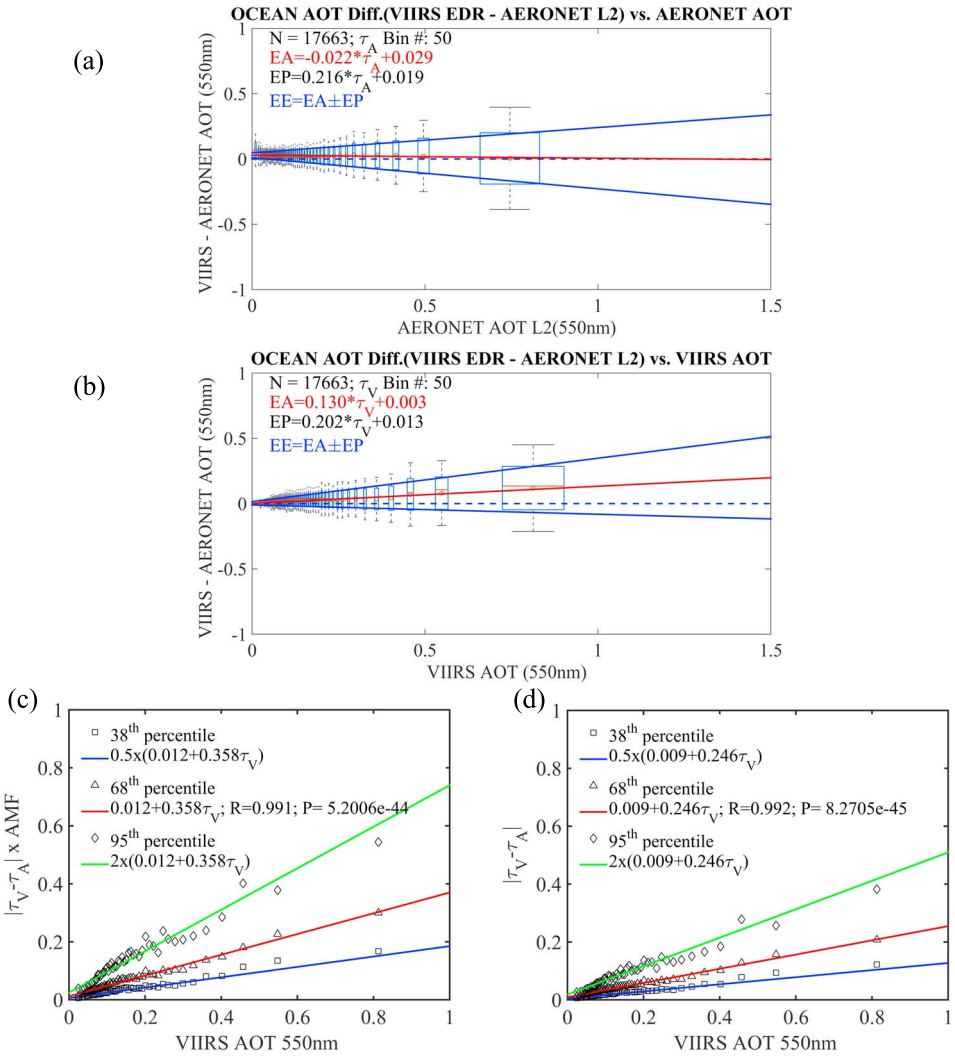

Figure 11. VIIRS Ocean AOT versus AERONET L2: (a) distribution of AOT difference between VIIRS AOT EDR and AERONET with dependence on AERONET AOT. (b) Distribution of the AOT difference between VIIRS AOT EDR and AERONET with dependence on VIIRS AOT. (c) The 38th (squares), 68th (triangles), and 95th (diamonds) sample percentiles of the AOT difference between VIIRS AOT EDR and AERONET as a function of VIIRS AOT, scaled by geometric AMF. (d) Same as Figure 11c but without being scaled by geometric AMF. Explanations of all the symbols and legends in Figures 11a–11d are the same in Figures 10a–10d.

2014 (excluding the processing error period of 15 October 2012 to 27 November 2012). In comparison to AERONET over land, the VIIRS AOT EDR exhibits an almost negligible global bias of −0.0008 with a global AOT mean of 0.17 and an uncertainty of 0.12. Without assuming a Gaussian distribution of absolute errors, the EE range can be estimated as a function of AERONET AOT ($-0.470\times\tau_A-0.010$, $-0.0058\times\tau_A+0.090$) or as a function of VIIRS AOT ($-0.249\times\tau_V-0.054$, $0.519\times\tau_V+0.010$). The mean bias changes from positive to negative with the increase of AERONET AOT ($EA=-0.238\times\tau_A+0.040$). Over ocean, globally, the mean difference between the VIIRS AOT EDR and AERONET is 0.0252 with a global AOT mean of 0.15 and an uncertainty of 0.065. Without assuming a Gaussian distribution of absolute errors, the EE range can be estimated as a function of AERONET AOT ($-0.238\times\tau_A+0.010$, $0.194\times\tau_A+0.048$) or as a function of VIIRS AOT ($-0.071\times\tau_V-0.010$, $0.332\times\tau_V+0.016$). The mean bias stays positive as the AERONET AOT increase until the AOT gets much higher ($EA=-0.022\times\tau_A+0.029$). These expected error estimations are comparable to the expected errors of the heritage satellite aerosol products. The expected errors of the MODIS Dark Target aerosol optical thickness (AOT) at 550 nm is ±0.03 ± 0.05AOT over ocean and ±0.05 ± 0.15AOT over land [*Levy et al.*, 2013]. The expected error of the MODIS Deep Blue AOT over land is estimated to be better than ±0.05 ± 20% AOT [*Hsu et al.*, 2013], and the same expected error is attributed to MISR AOT [*Kahn et al.*, 2010].

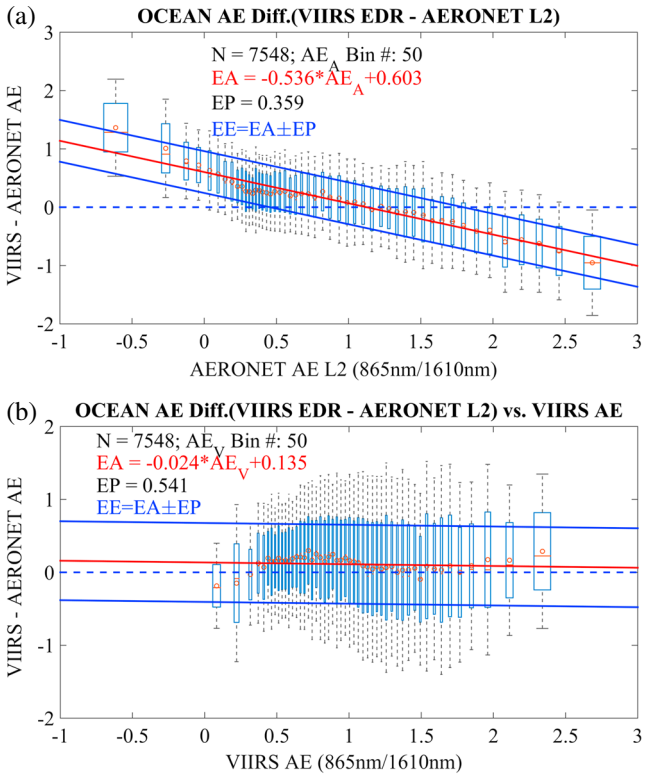

Figure 12. VIIRS Ocean AE versus AERONET L2: (a) distribution of AE difference between VIIRS AE EDR and AERONET with dependence on AERONET AEand (b) distribution of the AE difference between VIIRS AE EDR and AERONET with dependence on VIIRS AE.

In comparison to the preliminary evaluation results reported in *Liu et al.* [2014], this work showed that the VIIRS land AOT has lower bias (−0.0008 versus −0.009), lower precision (0.116 versus 0.130) and lower uncertainty (0.116 versus 0.130) than the earlier work. For ocean AOT, however, this study reported an almost doubled positive bias (0.025 versus 0.013) but comparable precision (0.060 versus 0.061) and uncertainty (0.065 versus 0.062). The almost doubled positive bias of ocean AOT was also confirmed from the VIIRS versus Maritime Aerosol Network (MAN) comparison for the same validation period (0.025 versus 0.013, results not shown). The differences in the statistics between the preliminary evaluation and this validation are attributable mainly to the following differences. First, *Liu et al.* [2014] used the more readily available AERONET L1.5 data sets while this work used the quality assured AERONET L2 data set. Second, this work extended the validation period 16 months longer than *Liu et al.* [2014] and thus more seasonal and interannual aerosol variabilities were accounted for in the statistics.

The VIIRS AE EDR agreed with the AERONET AE well with more positive bias at the lower bound (coarse particles) but negative bias at the higher bound (fine particles) ($EA = -0.536 \times AE_A + 0.603$). The expected error range for the VIIRS AE EDR over ocean was estimated as a function of logarithmic scale of AOT, $(-0.103 \times \log(\tau_A) - 0.566,\ -0.403 \times \log(\tau_A) + 0.020)$ as a function of AERONET AOT or $(0.057 \times \log(\tau_V) - 0.346,\ -0.385 \times \log(\tau_V) + 0.122)$ as a function of VIIRS AOT, with larger dependence on AOT rather than AE itself. Globally, the mean and standard deviation of the biases are 0.115 and 0.570, respectively, but they are reduced if only high AOT samples (i.e., AOT at 550 nm greater than 0.15) are used in the matchups.

Over land, the mean bias and retrieval uncertainty decrease when wavelengths increase, but correlation deteriorates significantly as the wavelength gets longer. Over ocean, however, the mean bias and retrieval uncertainty also decrease with the wavelengths increase, but its correlation remains high for longer wavelengths up to 865 nm. Thus, Ocean AE with spectral AOT at different pairs of wavelengths can be calculated as alternative particle size parameter to the operational AE that is calculated for only the wavelength pair 865 nm and 1610 nm.

The VIIRS AOT IP over land has higher positive bias and larger uncertainty than the VIIRS AOT EDR, but the VIIRS AOT IP and AE IP over ocean perform competitively with the VIIRS AOT and AE EDR.

VIIRS land AOT retrieval generally underestimates AOT over India and central Africa during agricultural burning seasons but overestimates AOT over Eastern U.S., the maritime continent and elsewhere. The link of the AOT biases to the biomass burning seasons over India and central Africa also warrants more in-depth data analysis in the land aerosol model characterization and the model selection process. The VIIRS biases also showed some association with the SWIR band-based Brightness Index and the NIR based $NDVI_{1240\ nm}$. The darker the surface or the higher the NDVI values, the more potential positive biases in the VIIRS AOT retrievals, although with reduced noise. The VIIRS Land AOT biases increase from negative to positive as vegetation cover and surface darkness increase, suggesting a more dynamic relationship exists between the spectral surface reflectance ratios and the land surface parameters than that which is currently employed in the algorithm.

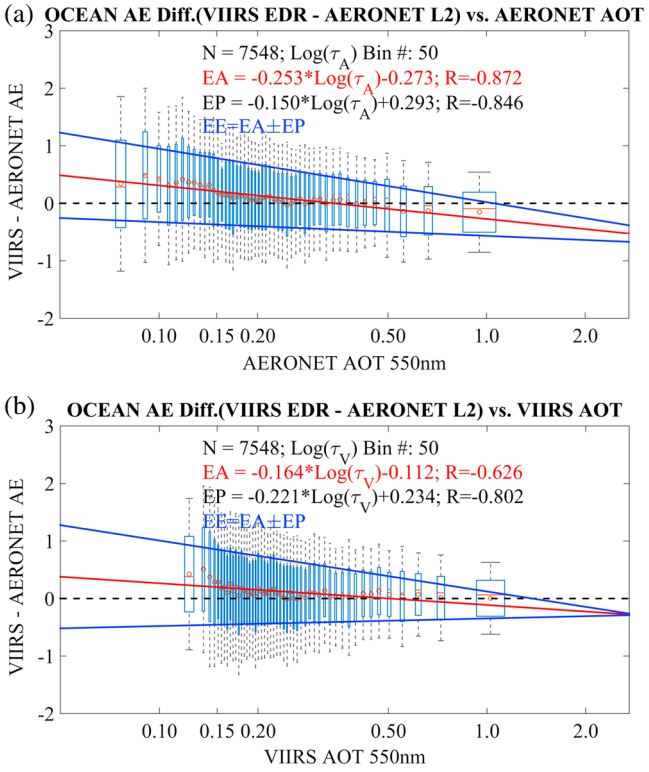

Figure 13. VIIRS Ocean AE versus AERONET L2: (a) distribution of AE difference between VIIRS AE EDR and AERONET with dependence on AERONET AOT and (b) distribution of the AE difference between VIIRS AE EDR and AERONET with dependence on VIIRS AOT.

No significant dependence of the AOT biases to solar and sensor viewing geometries was observed in the global statistics. Different land aerosol models exhibited different performance. The Dust and the Urban Clean models are the models in the VIIRS versus AERONET matchup selected most often, and the Urban Clean and the Smoke Low Absorption models have the largest positive biases and data uncertainty overall. The AOT bias seems to be more positive when the AERONET AE gets higher (more fine particles) while the land model selection seems to meet expectation when it is related to the AERONET AE: dust model is indeed more frequently selected when the AERONET AE is lower with higher coarse mode fraction.

For the validation of the VIIRS EDR products, the requirements on accuracy and precision from the NOAA JPSS Level 1 Requirements Document [*NOAA*, 2014] are listed in Table 3. There are no maturity evaluation requirements for the IP products. According to these requirements and the criteria for JPSS maturity level definitions (http://www.jpss.noaa.gov/science-maturity-level.html, accessed on 11 May 2016), the assessment results (see Table 3) show that the VIIRS AOT EDR over land reached Validated Stage II beginning 23 January 2013; the AOT EDR and AE EDR over ocean reached Validated Stages II and I, respectively, beginning 2 May 2012, excluding the processing error period 15 October to 27

Table 3. Evaluation of the Accuracy and Precision of the VIIRS AOT and AE EDR Against the JPSS L1RD Specification Thresholds[a]

Evaluation Condition	Accuracy or Precision	JPSS 1 Specification	VIIRS Aerosol EDR	Meet JPSS1 Specification
LAND AOT (23 January 2013 to 31 December 2014)				
AOT < 0.1	Accuracy	0.06	0.02	Yes
	Precision	0.15	0.06	Yes
0.1 ≤ AOT ≤ 0.8	Accuracy	0.05	−0.02	Yes
	Precision	0.25	0.11	Yes
0.8 < AOT ≤ 2.0	Accuracy	0.20	−0.20	Yes
	Precision	0.45	0.34	Yes
OCEAN AOT (02 May 2012 to 31 December 2014, excluding 15 October 2012 to 27 November 2012)				
AOT < 0.3	Accuracy	0.08	0.03	Yes
	Precision	0.15	0.04	Yes
0.3 ≤ AOT ≤ 2.0	Accuracy	0.15	0.02	Yes
	Precision	0.35	0.13	Yes
OCEAN AE (02 May 2012 to 31 December 2014, excluding 15 October 2012 to 27 November 2012)				
865 nm/1610 nm	Accuracy	0.30	0.12	Yes
	Precision	0.60	0.56	Yes

[a]The VIIRS Land AOT reached Validated Stage II maturity level on 23 January 2013. The VIIRS Ocean AOT and Ocean AE reached Validated Stage II and Validated Stage I maturity levels on 02 May 2012, respectively, but excluding the processing error period of 15 October 2012 to 27 November 2012.

November 2012. Validation of the VIIRS AOT and AE products with the quality assured AERONET Level 2.0 measurements with a much more extended data period demonstrates that VIIRS can provide a quantitative measure of aerosol optical thickness and particle size information representative of the real atmosphere, as measured by AERONET. The validated VIIRS AOT and AE data sets are ready for use by user communities and can be used for quantitative studies and applications in scientific publications. The findings from the validation and expected error estimation of the S-NPP VIIRS aerosol products will aid in the improvement of the VIIRS aerosol products as we transition from S-NPP to JPSS-1.

Acknowledgments

This study is supported by NOAA JPSS Program Office under a grant to the Cooperative Institute for Climate and Satellites—Maryland (CICS-Maryland). The authors would like to acknowledge the support from the following organizations for their assistance in the development of the VIIRS aerosol algorithm and the associated VIIRS aerosol calibration and validation work: NOAA JPSS program office (Mitchell D. Goldberg, JPSS Program Scientist and Lihang Zhou, JPSS STAR Program Manager), VIIRS SDR and VCM calibration and validation teams, NASA AERONET teams, NASA MAPSS team, and NASA Atmosphere PEATE at the University of Wisconsin. The authors thank the AERONET principal investigators and site managers who provided the data used in the validation analysis. The manuscript contents are solely the opinions of the authors and do not constitute a statement of policy, decision, or position on behalf of NOAA or the U.S. government. All the VIIRS data used in this study are publicly accessible at the NOAA Comprehensive Large Array-Data Stewardship System (http://www.class.ngdc.noaa.gov/). The AERONET data used in this study are publicly accessible at the AERONET Team website at NASA Goddard Space Flight Center (http://aeronet.gsfc.nasa.gov/). For any questions related to the VIIRS aerosol data set, please contact Istvan.Laszlo@noaa.gov or Shobha.Kondragunta@noaa.gov.

References

Aerosol ATBD (2015a), VIIRS aerosol optical thickness and particle size parameter algorithm theoretical basis document (Revision B): 474-00049. Effective Date: Jun, 2015. [Available at http://npp.gsfc.nasa.gov/sciencedocs/2015-06/474-00049_ATBD-VIIRS-AOT-APSP_C.pdf.]

Aerosol OAD (2015b), VIIRS aerosol products (AOT, APSP & SM) intermediate product (IP)/environmental data records (EDR) software - OAD (Revision F): 474-00073. Effective Date: September 2015. [Available at http://npp.gsfc.nasa.gov/sciencedocs/2015-09/474-00073_OAD-VIIRS-Aerosols-IP-EDR_H.pdf.]

Albrecht, B. (1989), Aerosols, cloud microphysics, and fractional cloudiness, *Science*, *245*, 1227–1230.

Boucher, O., et al. (2013), Clouds and Aerosols, in *Climate Change 2013: The Physical Science Basis. Contribution of Working Group I to the Fifth Assessment Report of the Intergovernmental Panel on Climate Change*, edited by T. F. Stocker, et al., pp. 571–658, Cambridge Univ. Press, Cambridge, U. K., and New York, doi:10.1017/CBO9781107415324.016.

Chin, M., R. A. Kahn and S. E. Schwartz (Eds.) (2009), *Atmospheric Aerosol Properties and Climate Impacts*, A Report by the U.S. Climate Change Science Program and the Subcommittee on Global Change Research, National Aeronautics and Space Administration, Washington, D. C., 128 pp.

Diner, D. J., et al. (2004), PARAGON: An integrated approach for characterizing aerosol climate impacts and environmental interactions, *Bull. Am. Meteorol. Soc.*, *85*, 1491–1501, doi:10.1175/BAMS-85-10-1491.

Eck, T. F., B. N. Holben, J. S. Reid, O. Dubovik, A. Smirnov, N. T. O'Neill, I. Slutsker, and S. Kinne (1999), Wavelength dependence of the optical depth of biomass burning, urban, and desert dust aerosols, *J. Geophys. Res.*, *104*(D24), 31,333–31,349, doi:10.1029/1999JD900923.

Ginoux, P., J. M. Prospero, T. E. Gill, N. C. Hsu, and M. Zhao (2012), Global-scale attribution of anthropogenic and natural dust sources and their emission rates based on MODIS Deep Blue aerosol products, *Rev. Geophys.*, *50*, RG3005, doi:10.1029/2012RG000388.

Gobbi, G. P., Y. J. Kaufman, I. Koren, and T. F. Eck (2007), Classification of aerosol properties derived from AERONET direct Sun data, *Atmos. Chem. Phys.*, *7*, 453–458, doi:10.5194/acp-7-453-2007.

Goldberg, M. (2013), Joint Polar Satellite System: The United States next generation civilian polar orbiting environmental satellite system, *J. Geophys. Res. Atmos.*, *118*, 13,463–13,475, doi:10.1002/2013JD020389.

Guo, J. P., M. Deng, S.-S. Lee, F. Wang, Z. Li, P. Zhai, H. Liu, W. Lv, W. Yao, and X. Li (2015), Delaying precipitation and lightning by air pollution over the Pearl River Delta. Part I: Observational analyses, *J. Geophy. Res. Atmos.*, doi:10.1002/2015JD023257.

Hand, J. L., et al. (2011), Spatial and seasonal patterns and temporal variability of haze and its constituents in the United States: Report V, June (2011). [Available at http://vista.cira.colostate.edu/improve/Publications/Reports/2011/2011.htm.]

Holben, B. N., et al. (1998), AERONET - A federated instrument network and data archive for aerosol characterization, *Remote Sens. Environ.*, *66*(1), 1–16, doi:10.1016/S0034-4257(98)00031-5.

Hsu, N. C., M.-J. Jeong, C. Bettenhausen, A. M. Sayer, R. Hansell, C. S. Seftor, J. Huang, and S.-C. Tsay (2013), Enhanced Deep Blue aerosol retrieval algorithm: The second generation, *J. Geophys. Res. Atmos.*, *118*, 9296–9315, doi:10.1002/jgrd.50712.

Huang, J., D. Chen, and M. Cosh (2009), Sub-pixel reflectance unmixing in evaluating vegetation water content and dry biomass of corn and soybeans cropland using normalized difference water index (NDWI) from satellites, *Int. J. Remote Sens.*, *30*(8), 2075–2104.

Huang, J., C. Zhang, and J. M. Prospero (2010), African dust outbreaks: A satellite perspective of temporal and spatial variability over the tropical Atlantic Ocean, *J. Geophys. Res.*, *115*, D05202, doi:10.1029/2009JD012516.

Jackson, J., H. Liu, I. Laszlo, S. Kondragunta, L. A. Remer, J. Huang, and H. Huang (2013), Suomi-NPP VIIRS aerosol algorithms and data products, *J. Geophys. Res. Atmos.*, *118*, 12,673–12,689, doi:10.1002/2013JD020449.

Kahn, R. A., B. J. Gaitley, M. J. Garay, D. J. Diner, T. F. Eck, A. Smirnov, and B. N. Holben (2010), Multiangle Imaging SpectroRadiometer global aerosol product assessment by comparison with the Aerosol Robotic Network, *J. Geophys. Res.*, *115*, D23209, doi:10.1029/2010JD014601.

Kaufman, Y. J., D. Tanre, L. A. Remer, E. F. Vermote, A. Chu, and B. N. Holben (1997), Operational remote sensing of tropospheric aerosol over land from EOS moderate resolution imaging spectroradiometer, *J. Geophys. Res.*, *102*(D14), 17,051–17,067, doi:10.1029/96JD03988.

Kaufman, Y. J., D. Tanré, and O. Boucher (2002), A satellite view of aerosols in the climate system, *Nature*, *419*, 215–223, doi:10.1038/nature01091.

King, M. D., Y. J. Kaufman, D. Tanré, and T. Nakajima (1999), Remote sensing of tropospheric aerosols from space: Past, present and future, *Bull. Am. Meteorol. Soc.*, *80*, 2229–2259.

Koren, I., and G. Feingold (2011), Aerosol-cloud-precipitation system as a predator-prey problem, *Proc. Natl. Acad. Sci. U.S.A.*, *108*, 12,227–12,232, doi:10.1073/pnas.1101777108doi:10.1073/pnas.1101777108.

Koren, I., O. Altaratz, L. A. Remer, G. Feingold, J. V. Martins, and R. Heiblum (2012), Aerosol-induced intensification of rain from the tropics to the mid-latitudes, *Nat. Geosci.*, *5*, 118–122, doi:10.1038/ngeo1364.

Kotchenova, S. Y., and E. F. Vermote (2007), Validation of a vector version of the 6S radiative transfer code for atmospheric correction of satellite data. Part II. Homogeneous lambertian and anisotropic surfaces, *Appl. Opt.*, *46*(20), 4455–4464, doi:10.1364/ao.46.004455.

Kotchenova, S. Y., E. F. Vermote, R. Matarrese, and F. J. Klemm (2006), Validation of a vector version of the 6S radiative transfer code for atmospheric correction of satellite data. Part I: Path radiance, *Appl. Opt.*, *45*(26), 6762–6774, doi:10.1364/ao.45.006762.

Lau, K., M. Kim, and K. Kim (2006), Asian summer monsoon anomalies induced by aerosol direct forcing—The role of the Tibetan Plateau, *Clim. Dyn.*, *36*, 855–864, doi:10.1007/s00382-006-10114-z.

Levy, R. C., L. A. Remer, S. Mattoo, E. F. Vermote, and Y. J. Kaufman (2007), Second-generation operational algorithm: Retrieval of aerosol properties over land from inversion of Moderate Resolution Imaging Spectroradiometer spectral reflectance, *J. Geophys. Res.*, *112*, D13211, doi:10.1029/2006JD007811.

Levy, R. C., L. A. Remer, R. G. Kleidman, S. Mattoo, C. Ichoku, R. Kahn, and T. F. Eck (2010), Global evaluation of the Collection 5 MODIS dark-target aerosol products over land, *Atmos. Chem. Phys.*, *10*, 11,0399–10,420, doi:10.5194/acp-10-10399-2010.

Levy, R. C., S. Mattoo, L. A. Munchak, L. A. Remer, A. M. Sayer, and N. C. Hsu (2013), The Collection 6 MODIS aerosol products over land and ocean, *Atmos. Meas. Tech. Discuss.*, *6*, 159–259, doi:10.5194/amtd-6-159-2013.

Liu, H., L. A. Remer, J. Huang, H. Huang, S. Kondragunta, I. Laszlo, M. Oo, and J. Jackson (2014), Preliminary evaluation of S-NPP VIIRS aerosol optical thickness, *J. Geophys. Res. Atmos.*, *119*, 3942–3962, doi:10.1002/2013JD020360.

Lohmann, U., and J. Feichter (2005), Global indirect aerosol effects: A review, *Atmos. Chem. Phys.*, *5*, 715–737.

Martin, R. V., D. J. Jacob, R. M. Yantosca, M. Chin, and P. Ginoux (2003), Global and regional decreases in tropospheric oxidants from photochemical effects of aerosols, *J. Geophys. Res.*, *108*(D3), 4097, doi:10.1029/2002JD002622.

Myhre, G., et al. (2005), Intercomparison of satellite retrieved aerosol optical depth over ocean during the period September 1997 to December 2000, *Atmos. Chem. Phys.*, *5*, 1697–1719.

NOAA (2014), Joint Polar Satellite System (JPSS) Program Level 1 Requirements Document (L1RD) Supplement JPSS-REQ-1002 i. Version: 2.10. [Available at http://www.jpss.noaa.gov/pdf/L1RDS_JPSS_REQ_1002_NJO_v2.10_100914_final-1.pdf.]

Petrenko, M., C. Ichoku, and G. Leptoukh (2012), Multi-sensor Aerosol Products Sampling System (MAPSS), *Atmos. Meas. Tech.*, *5*, 913–926, doi:10.5194/amt-5-913-2012.

Pope, C. A., III, R. T. Burnett, M. J. Thun, E. E. Calle, D. Krewski, K. Ito, and G. D. Thurston (2002), Lung cancer, cardiopulmonary mortality, and long-term exposure to fine particulate air pollution, *J. Am. Med. Assoc.*, *287*, 1132–1141, doi:10.1001/pubs.JAMA-ISSN-0098-7484-287-9-joc11435.

Ramanathan, V., P. J. Crutzen, J. T. Kiehl, and D. Rosenfeld (2001), Aerosols, climate and the hydrological cycle, *Science*, *294*, 2119–2124.

Remer, L. A., and Y. J. Kaufman (1998), Dynamic aerosol model: Urban/industrial aerosol, *J. Geophys. Res.*, *10*(D12), 13,859–13,871, doi:10.1029/98JD00994.

Remer, L. A., et al. (2005), The MODIS aerosol algorithm, products, and validation, *J. Atmos. Sci.*, *62*, 947–973, doi:10.1175/JAS3385.1.

Remer, L. A., et al. (2008), Global aerosol climatology from the MODIS satellite sensors, *J. Geophys. Res.*, *113*, D14S07, doi:10.1029/2007JD009661.

Remer, L. A., D. Tanre, Y. J. Kaufman, R. Levy, and S. Mattoo (2009), Algorithm for remote sensing of tropospheric aerosol from MODIS for Collection 005: Revision 2 Products: 04_L2, ATML2, 08_D3, 08_E3, 08_M3.

Rosenfeld, D., U. Lohmann, G. B. Raga, C. D. O'Dowd, M. Kulmala, S. Fuzzi, A. Reissell, and M. O. Andreae (2008), Flood or drought: How do aerosols affect precipitation?, *Science*, *321*, 1309–1313, doi:10.1126/science.1160606.

Sayer, A. M., N. C. Hsu, C. Bettenhausen, and M.-J. Jeong (2013), Validation and uncertainty estimates for MODIS Collection 6 "Deep Blue" aerosol data, *J. Geophys. Res. Atmos.*, *118*, 7864–7872, doi:10.1002/jgrd.50600.

Smirnov, A., B. N. Holben, T. F. Eck, O. Dubovik, and I. Slutsker (2000), Cloud screening and quality control algorithms for the AERONET database, *Remote Sens. Environ.*, *73*, 337–349.

Streets, D. G., et al. (2003), An inventory of gaseous and primary aerosol emissions in Asia in the year 2000, *J. Geophys. Res.*, *108*(D21), 8809, doi:10.1029/2002JD003093.

Tanré, D., Y. J. Kaufman, M. Herman, and S. Mattoo (1997), Remote sensing of aerosol properties over oceans using the MODIS/EOS spectral radiances, *J. Geophys. Res.*, *102*(D14), 16,971–16,988, doi:10.1029/96JD03437.

Twomey, S. (1977), The influence of pollution on the shortwave albedo of clouds, *J. Atmos. Sci.*, *34*, 1149–1152.

Vermote, E. F., and S. Kotchenova (2008), Atmospheric correction for the monitoring of land surfaces, *J. Geophys. Res.*, *113*, D23S90, doi:10.1029/2007JD009662.

Vermote, E. F., D. Tanré, J. L. Deuzé, M. Herman, and J. J. Morcette (1997), Second simulation of the satellite signal in the solar Spectrum, 6S: An overview, *IEEE Trans. Geosci. Remote Sens.*, *35*, 675–686.

Yang, P., Q. Feng, G. Hong, G. W. Kattawar, W. J. Wiscombe, M. I. Mishchenko, O. Dubovik, I. Laszlo, and I. N. Sokolik (2007), Modeling of the scattering and radiative properties of nonspherical dust-like aerosols, *J. Aerosol Sci.*, *38*(10), 995–1014, doi:10.1016/j.jaerosci.2007.07.001.

Yu, H., L. A. Remer, R. A. Kahn, M. Chin, and Y. Zhang (2013), Satellite perspective of aerosol intercontinental transport: From qualitative tracking to quantitative characterization, *Atmos. Res.*, *124*, 73–100, doi:10.1016/j.atmosres.2012.12.013.

Yu, H., et al. (2015), The fertilizing role of African dust in the Amazon rainforest: A first multiyear assessment based on CALIPSO lidar observations, *Geophys. Res. Lett.*, *42*, 1984–1991, doi:10.1002/2015GL063040.

Zhang, J., J. R. Campbell, E. J. Hyer, J. S. Reid, D. L. Westphal, and R. S. Johnson (2014), Evaluating the impact of multi-sensor data assimilation on a global aerosol particle transport model, *J. Geophys. Res. Atmos.*, *119*, 4674–4689, doi:10.1002/2013JD020975.